Reconfigurable Fully Constrained Cable Driven Parallel Mechanism for Avoiding Interference between Cables

Khaled Youssef[1], Martin J.-D. Otis[2]

[1] Applied science department, University of Québec at Chicoutimi, Quebec, Canada: Khaled-mohamed.youssef1@uqac.ca

[2] Applied science department, University of Québec at Chicoutimi, Quebec, Canada: Martin_Otis@uqac.ca

Abstract

Cable driven parallel mechanisms (CDPMs) have attracted much attention due to their many advantages over conventional parallel mechanisms, such as the significantly large workspace and the dynamics capacity. One of the main issues involved in designing CDPMs is avoiding cable-cable collision, especially when an operator is sharing the same workspace with the moving parts of the mechanism. This paper aims to model and simulate a reconfigurable fully constrained CDPM and solve the forward and inverse kinematics given that the attachment points on the rails move up and down in real time, unlike conventional CDPMs where the attachment points are firmly fixed on specific positions on the rails. The new idea of reconfiguration is then used to avoid interference between two cables in real time by moving one cable's attachment point on the frame to increase the shortest distance between them while keeping the trajectory of the end effector unchanged. This new approach was tested by creating a simulated intended cable interference trajectory, hence detecting and avoiding cable collision using the proposed real time reconfiguration while maintaining the end effector trajectory.

1 Introduction

Parallel mechanisms have many advantages over serial ones. The closed chain kinematics of parallel mechanisms can result in greater structural rigidity and, therefore, greater accuracy compared with open chain manipulators [1]. Cable driven parallel mechanisms (CDPMs) are a new category of parallel mechanisms in which the end effector's pose (position and orientation) is manipulated by means of taut cables with negligible mass that can be extended or shortened using rotational motors (reels), and these motors are firmly attached to stationary rails. In addition to their advantages as parallel manipulators, they are also characterized by significantly large workspaces and dynamics capacity compared with conventional parallel mechanisms [2]. Moreover, they have lower mass compared with other parallel mechanisms due to the fact that the actuating links are replaced by cables, which leads to a higher payload to weight ratio.

Due to their better capabilities compared with conventional parallel mechanisms, CDPMs have been used in many applications, such as pick-and-place (to lift and transport heavy parts from one position to another) [3], haptic machines and locomotion interfaces [4], air vehicle simulator [5] and high-speed manipulators [6]. CDPMs are classified according to the number of cables and degree of freedom of the end effector [7]. In the first category, the mechanism is fully constrained if the number of cables is greater than the degrees of freedom of the end-effector. In the second category, the mechanism is under constrained if the number of cables is less than or equal to the degrees of freedom of the end-effector [8]. Since CDPMs were presented in the late 1980s, a wide variety of scientific research has been conducted to resolve issues and challenges related to such unique mechanism. Researchers in this field have addressed many problems, such as dynamic trajectory planning [9], kinematics study [10], workspace analysis [11], vibration analysis [12], control of the cables [4,13] and collisions between cables [14], with the environment, or with the mobile platform [15].

The inverse kinematics problem of CDPM can be defined as determining the cable lengths given the pose (position and orientation) of the end-effector. Due to the easiness of this problem in parallel mechanisms compared with serial ones, it has been studied and solved in many studies. Roberts [15] studied kinematics, statics, and fault tolerance [16] of cable suspended robots. The author illustrated some examples to demonstrate his approach for solving full inverse kinematics of CDPM driven by eight cables. Zi et al. [17] studied the dynamic modeling and active control of a cable-suspended parallel robot based on inverse kinematics analysis using Lagrange's equations. The authors proved the effectiveness of the proposed method by comparing experimental and simulation results. In addition, the control system was simple and fast, which is applicable to online applications. The dynamic model of a six-cable mechanism was formulated with non-negligible cable mass, and then a simulation of random wind forces was performed. In order to control wind-induced vibration, a fuzzy plus proportional–integral controller was suggested. However, the authors did not present any work on the forward kinematics or the effectiveness of the proposed model on a fully constrained cable driven mechanism.

Aref et al. [18] studied the cable to cable, cable to body and cable to work piece collisions of a six degrees of freedom cable driven redundant manipulator. The study was based on designing a full force feasible mechanism for the entire workspace, and then the workspace boundaries were determined by collision free algorithm. The authors demonstrated that this approach is practical for real time applications since its analysis takes less computational time. Meziane et al. [19] presented a new approach for preventing collisions between cables for CDPM driven by seven cables using admittance control during a human physical interaction. This approach depends on changing the trajectory of the mobile platform when a collision or near collision between two cables is detected. When an interference is close to happening, the user feels a virtual force that pushes the mobile platform in the inverse direction to increase the distance between the two interfering cables, and this direction is determined by a gradient vector. Therefore, the desired trajectory is not respected. Moreover, since it is possible to use an interference point as a virtual reel by crossing cables together as suggested in Wischnitzer et al. [20], it is also possible to maintain the desired trajectory. However, the non-linear behavior of friction at the interference point reduces the accuracy of the rendered force and torque at the end effector. The challenge is to keep the desired trajectory without reducing the rendered force and torque by a compromise on the size of the workspace. In order to maintain and continue the desired trajectory, the paper proposes moving the interference location. Therefore, our suggested solution considers a linear displacement of the reel position with the compromise of adapting the geometry and the workspace of the CDPM. The contribution of the present work is that the initial trajectory is unchanged. In a collaborative physical human-robot interaction, or in a haptic application [19], the trajectory comes from the user input and should not be constrained by cable interference to let the user perform its work or task using the CDPM. Otherwise, the trajectory is changed since the user is constrained by a force to avoid folding cables. Therefore, moving the reel position to avoid cable interference enables transparent manipulation.

Section 2 presents previous research on cable collision detection and avoidance. Sections 3, 4, 5 and 6 discuss the main contribution of this paper: solving the forward and inverse kinematics of a six degrees of freedom mechanism driven by eight cables given that the attachment points on the rails move vertically up and down, unlike conventional CDPM. Then, the new reconfiguration is used to detect and eliminate the interference between cables while maintaining the end effector trajectory.

2 Related work

Since the mobile platform is being manipulated by cables such that all the cables will always remain inside the geometry of the mechanism (installation space) and may be within the workspace [21], a collision investigation should be performed when designing such mechanism to ensure a collision-free workspace [22]. A collision may occur between cables, between cables and the environment, between the platform and the environment as well as between cables and the platform, as mentioned by Nguyen [23]. Bordalba et al. [24] proposes the use of a randomized kinodynamic planning technique to synthesize dynamic motions for cable-suspended parallel robots. The authors presented a method to find a collision-free trajectory [25,26] between two

points with known positions and velocities while maintaining the cables in tension continually and at the same time adhering to the actuators and joints force capabilities. The authors validated the proposed approach by experimental data on a specific cable driven mechanism design; they concluded that this approach is valid for other mechanism designs. Makino et al. [27] introduced a new design of six degrees of freedom with eight cables driven mechanism by embedding a rotational mechanism inside the moving part (end effector) and the cables are attached to it. A control algorithm is created to avoid collisions of cables when detected by changing the configurations of the cables by rotating the end effector around the vertical axis while rotating the pulley with the same amount of angle but in the opposite direction. However, the authors did not present any study on the computational time needed for the proposed approach and if it is valid for high-speed applications. Otis et al. [28] presented a determination and management method for cable interference between two 6 DOF foot platforms in a cable-driven locomotion interface. The presented method computes the cable interference geometrically for any constrained trajectory and, an algorithm determines which cable can be released from an active actuation state while maintaining all the other cables in tension. The authors also solved the tension discontinuity issue that arises from releasing a cable from an active actuation state by presenting a collision prediction scheme that is applied to redundant actuators. The limitation of the workspace is the main issue arising from folding two cables on each other. Perreault et al. [29] proposed a method to optimize the workspace space given a prescribed workspace by locating the reel position while considering interference regions between two cables and/or between a cable and the end effector edges. However, the authors suggested that a free interference trajectory can be planned using the predetermined regions, which makes this approach valid for only limited trajectories. Wischnitzer et al. [20] suggested a method to permit collisions between cables for the sake of expanding the workspace significantly compared with collision free workspace mechanisms. The presented method was based on formulating the inverse kinematics of a six degrees of freedom redundant robot with two colliding cables and solving numerically while maintaining a feasible and positive wrench closure. Experimental and theoretical results were presented, and they demonstrated workspace expansion compared with a collision free case. However, the authors did not present any study on the vibration issue resulting from colliding cables, especially in high-speed applications. Ismail et al. [30] presented a dynamic path planning [31,32] algorithm for an under constrained planar mechanism to find the shortest path between two points while maintaining the wrench feasible workspace and at the same time avoiding obstacles. The algorithm was originally created for a serial manipulator; however, it was adapted for the proposed hybrid planar design. The authors did not discuss if the proposed approach is valid for spatial mechanisms. Pinto et al. [33] presented a four degrees of freedom wire driven mechanism called SPIDERobot, which was designed for industrial pick and place applications. A new approach is introduced to optimize the trajectory of the robot by means of visual interpretation of the workspace. The suggested method is based on visually locating the position of the robot, its destination and the obstacles. This method determines the trajectory while avoiding the collision of the cables with the environment. The authors concluded that the approach is valid and effective for under constrained cable mechanisms by presenting simulated models; however, they did not include any examples for fully constrained parallel mechanisms.

Zhou et al. [34] added a new classification for cable driven manipulators: The first type is the conventional cable driven mechanism where the base is fixed and the mobile platform is controlled by varying the cable lengths, and the second type has the cable lengths fixed and the base moved to manipulate the mobile platform. In his study [34], Zhou combined the two types of cable driven mechanisms. However, he only discussed a three degrees of freedom mechanism derived by four cables. The authors concluded that for a given trajectory, adding a mobile base extends the wrench closure workspace as well as optimizes the tension factor for a better wrench feasible workspace. In 2017, Anson et al. [35] conducted another study on adding a mobile base for cable driven mechanism. However, it was also a planar three degrees of freedom mechanism driven by four cables. The authors investigated the quality of the wrench closure workspace by a tension factor index approach by comparing a traditional cable driven mechanism with a mobile base one. Two configurations were used in the study. The first type has a rectangular base and each attachment point is constrained to move along its own linear rails. In the second type, the attachment points were constrained to move along a circular base. The authors concluded that the circular base had the better wrench closure workspace where the mobile platform had the ability to reach any position and orientation within the installation workspace. Tourajizadeh et al. [36] presented an optimal regulation for an under constrained six degrees of freedom mechanism driven by six cables to maximize the dynamic load capacity of the mobile platform for a

predefined path while avoiding cables interference. However, in case of a near collision between two cables, the orientation of the mobile platform is changed to avoid interference, which makes this approach not valid for some applications that require vertical movements, such as pick-and-place. Table 1 is a summary about the pros and cons of previous research in the field of cables collision interference and avoidance.

	Current study				
	6	8	Yes	Yes	-Online computation. -Detect near cable collision and provide solution to avoid it. -Initial trajectory is unchanged. -Applicable for any architecture. -Present solution when reaching mechanical limit of the attachment points. -Workspace analysis due to reconfiguration. -Smooth transition in all cable tension values since no cable is released. -Spatial mechanism. -Cables interference detection and avoidance is presented and simulated.
Reference	Degrees of freedom	Number of cables	Workspace analysis	Trajectory preserved	Comments
Bordalba et al. (2018)	3	3	No	No	-Validated for specific architectures only.
Makino et al. (2016)	6	8	No	No	-End effector orientation is changed to avoid cable collision. -Did not present solutions if mechanical limit of rotating pulley is reached. -No workspace discussion due to reconfiguration.
Otis et al. (2009)	6	8	No	Yes	-Limited workspace due to release of one cable. -Approach may lead to generation of mechanical vibration and instability due to sudden increase in other cables' tension.
Perreault et al. (2010)	6	8	No	No	-Offline computation. -Computes all planes at which interference between two cables can occur but do not give solution to avoid cable collision. -Valid for predetermined trajectories only

Reference	Degrees of freedom	Number of cables	Workspace analysis	Trajectory preserved	comments
Wischnitzer et al. (2008)	6	7	yes	no	-No vibration analysis due to collision permit. -Discuss the permit of two cables only without giving consequences in case of more than two-cable collision. -Neglect the friction at the point of contact between two cables.
Ismail et al. (2016)	2	2	no	no	-Planar mechanism. -Hybrid cable–serial robot. -Predetermined specific trajectories that avoid obstacles.
Pinto et al. (2017)	3	4	no	no	-Predetermined free collision trajectory depending on visual images of the workspace. -No wrench or feasible workspace analysis.
Anson et al. (2017)	3	4	yes	no	-Planar mechanism (2D) -Wrench closure workspace analysis due to reconfiguration -No study was conducted on cable interference avoidance.
Tourajizadeh et al. (2016)	6	6	No	No	-Orientation of the mobile platform is deviated to avoid cable interference.

Table 1. Comparison between current and previous studies in terms of degrees of freedom, number of cables, workspace and trajectory

3 Suggested simulation model

This section discusses the modeling analysis of CDPM by symbolically establishing the coordinate system and the kinematic constraints due to the translational joints as well as the driving constraints. The suggested model is six degrees of freedom mechanism driven by eight cables. The model is designed such that the upper attachment point on the rail is attached to the lower point on the mobile platform (crossed cable design). This arrangement of attachment points allows a better control in rotation; hence, it is a tradeoff between control and interference between cables. Our proposed configuration is then used to detect and avoid cable collision while keeping the end effector trajectory unchanged.

3.1 Coordinate system and kinematics constraints

In our study, a fixed global frame (X-Y-Z) is set at the bottom left corner with the Z axis pointing vertically upward and the X-Y axes are set according to the right hand rule as shown in Figure 1. The mechanism consists of eight attachment points (A_i) that can move vertically up and down on four fixed rails and at the same time control the lengths of eight cables (In real implementation, the motors can be fixed on the ground and only the attachment points can be relocated by means of a pulley). The eight cables are attached (B_i) to the mobile end effector (in the shape of a rectangular prism) to manipulate its pose (position and orientation) by extending and shortening the cables (ρ_i). The generalized coordinates ($\vec{q}$) of the mechanism consist of the following:

$$\vec{q} = [(\vec{q}_{er})^T, (\vec{q}_{ac})^T]^T, \quad (1)$$

$$\text{where } \left\{ \begin{matrix} \vec{q}_{er} = [x_p, y_p, z_p, \theta_p, \beta_p, \gamma_p] \\ \vec{q}_{ac} = [x_i, y_i, z_i] \end{matrix} \right\}, \text{ for } i = 1 \text{ to n} \quad (2)$$

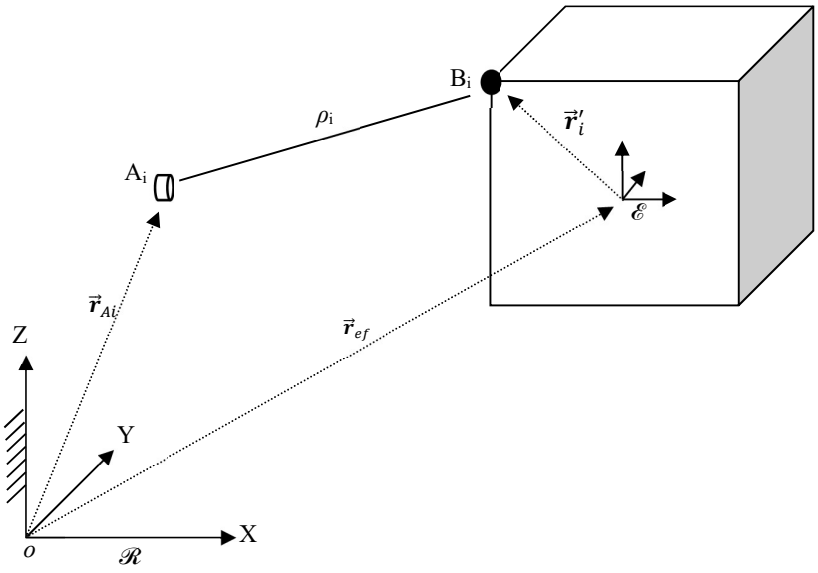

Figure 1. kinematic diagram

where $\vec{q}_{ac}$ and $\vec{q}_{er}$ are the generalized coordinates of the attachment points on the rail and end effector respectively and n is the number of cables. The kinematic constraints are defined as the constraints formed by the joints connecting rigid bodies [37]. In this model, the kinematics constraints can be described as the restrictions of the eight attachment points to move only in the vertical direction (i.e., they cannot move in the x or y direction as they are restricted by the rails). This can be formulated mathematically as follows:

$$\begin{bmatrix} x_i \\ y_i \end{bmatrix} = \begin{bmatrix} k_i^1 \\ k_i^2 \end{bmatrix} \; for\; i = 1 \text{ to n}, \tag{3}$$

where x_i and y_i are the Cartesian coordinates of point A_i defined in the global coordinate system, and k is a constant based on the position of each attachment point with respect to the fixed global frame.

3.2 Driving constraints

The driving constraints, as described by Shabana [38], are the specified motion trajectories, which may depend on the system's generalized coordinates [37] and time. In our mechanism, the driving constraints consist of two groups. In the first group, driving constraints formulations are due to the vertical motion of the eight attachment points on the rails, while in the second group, they are due to the extension and retraction of the eight cables attached to the end effector. The first driving constraint group can be mathematically represented as follows:

$$z_i = c_i(t, \vec{q}), \quad \text{for } i = 1 \text{ to n}, \tag{4}$$

where z_i is the z coordinate of each attachment point A_i represented in the global coordinate system, and $c_i(t,\vec{q})$ is the imposed function that drives the attachment point vertically and may be time and/or generalized coordinates ($\vec{q}$) dependent. The formula of the second group of driving constraints is defined as change in the length of the eight cables (ρ_i). This constraint is shown in Figure 2, where the length of the cable will always be the hypotenuse of a right angle triangle formed by the vertices A_1, B_1 and B_{1z}. This constraint can be represented mathematically as follows:

$$(B_x)_i^2 + (B_y)_i^2 + (A_i - (B_z)_i)^2 = \rho_i^2, \quad \text{for } i = 1 \text{ to n}. \tag{5}$$

The coordinates of point B_i can be represented as follows:

$$\vec{r}_{ef} + \boldsymbol{R}\vec{r}'_i, \text{for } i = 1 \text{ to n}, \tag{6}$$

where $\vec{r}_{ef}$ is the position vector of the center of mass of the end effector, and $\boldsymbol{R}$ is the rotation matrix following

XYZ convention. $\vec{r}'_i$ is the local coordinate of the 8 vertices of the rectangular prism represented in the local coordinate frame attached to the mobile end effector $\mathscr{E}$.

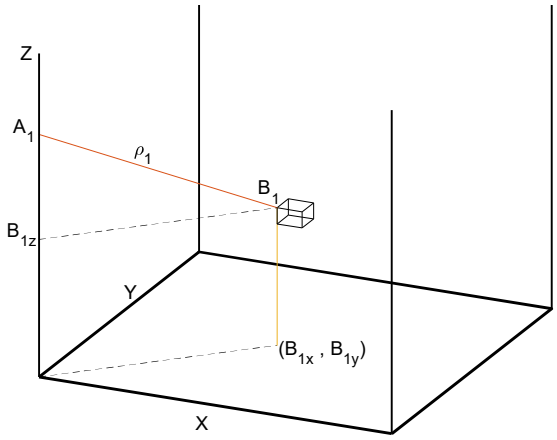

Figure 2. Geometry of second group of driving constraints

The total kinematic constraint (KC) equations are as follows:

$$\varphi = \begin{bmatrix} x_i - k_i^1 \\ y_i - k_i^2 \\ z_i - c_i(t, \vec{q}) \\ (\mathrm{B}_x)_i^2 + (\mathrm{B}_y)_i^2 + (\mathrm{A}_i - (\mathrm{B}_z)_i)^2 - (\rho_i)^2 \end{bmatrix}, \quad \text{for } i = 1 \text{ to n.} \tag{7}$$

3.3 Crossed cable configuration

The crossed configuration of the mobile platform attachment points is shown in Figure 3, where the original configuration has been changed so that the upper attachment points on the rail are connected to the lower anchor points on the mobile platform and vice versa. The crossed cable configuration allows a better orientation workspace and stiffness map [8]. Figure 3 shows a schematic for the mobile platform, where $\mathscr{E}$ is a local frame attached to the mobile platform at its center of mass. The mobile platform dimensions are 0.5×0.5×0.5 m3. The locations of the anchor points on the mobile platform are shown in Table 2 with respect to the local frame $\mathscr{E}$ in meters. In order to evaluate the presented approach, three different trajectories of the mobile platform are chosen such that the Z-height of the end effector is constant as well as its orientation (i.e. the mobile platform will perform a rectilinear and/or curvilinear translation for the three different trajectories). In order for the reader to be able to replicate the results, the three trajectories will be provided in appendix A in form of Cartesian coordinates of the center of mass of the end effector. The suggested trajectories will be confirmed to lie within the feasible closure workspace by computing and plotting the tension values within the eight cables. Hence, Section 5.1 is dedicated to establishing the necessary formulas to solve for the tension distribution of the eight cables.

	B_1	B_2	B_3	B_4	B_5	B_6	B_7	B_8
x	-0.15	-0.25	-0.15	-0.25	0.15	0.25	0.15	0.25
y	-0.25	-0.15	0.25	0.15	0.25	0.15	-0.25	-0.15
z	-0.25	0.25	-0.25	0.25	-0.25	0.25	-0.25	0.25

Table 2. Local positions of the eight anchor points (meters)

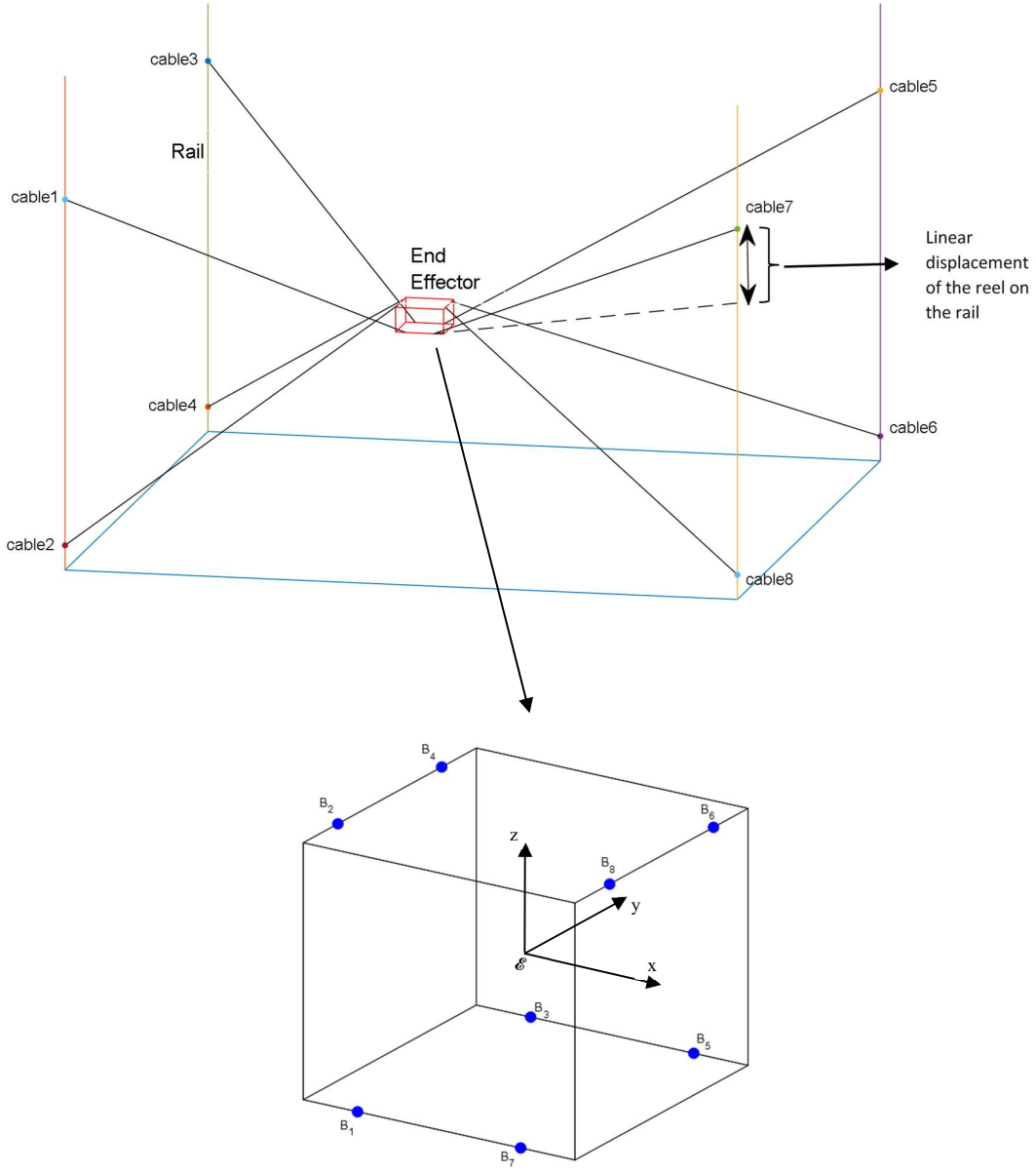

Figure 3. Arrangement of attachment points on the rails and mobile platform

4 Forward and inverse kinematics

Contrary to the inverse kinematics, the forward kinematics of CDPM is determining the position and orientation of the movable end-effector given the lengths of the actuated cables. Forward kinematics is a very important step in closed loop position control of parallel mechanisms. Forward kinematics of CDPM, unlike serial manipulators, has no known closed form solution for the most general CDPM [39]. The fully constrained mechanism is similar in geometry and construction to the Stewart Gough mechanism (SGm), but the difference is that SGm consists of a fixed base plate and a mobile upper plate that are connected together with six extensible rigid rods. Due to this similarity, the approaches used to solve the forward kinematics of SGm [40] is applicable to solve fully constrained CDPM. Husty [41] introduced a method for solving the forward kinematics problem of 6-6 SGm with a minimal set of constrained equations obtained by kinematic mapping to produce a univariate polynomial of 40th degree. In this method, the parallel manipulator kinematics is formulated as a polynomial equation system where the number of equations is equal to the number of unknowns. As stated by the author, in solving the most general case (6-6

Stewart platform), the rational representation comprised a univariate equation of degree 40, and 4 real solutions were computed. Obviously, this approach is not suitable for real time applications due to its computational burden and multiple solutions. Pott [10] presented an algorithm for solving real time forward kinematics of CDPM using a combination of interval techniques and an iterative solver; the author validated his approach by applying it experimentally on a seven-cable parallel robot. Liwen et al. [42] solved the forward kinematics of six-cable parallel mechanism (fully constrained) by finding the end-effector pose using minimum potential energy principle. Ghasemi et al. [39] solved the forward kinematics using multilayer perceptron (Artificial Neural Network) method. The authors demonstrated higher modeling accuracy compared with other approaches; however, they did not study the required convergence time for such lengthy computations, but the convergence time is very important for high-speed applications. In order to control a mechanism, the forward kinematics issue has to be solved first. In our study, unlike conventional CDPM, the eight attachment points on the rails move vertically. The main issue with the kinematics problem in this model is that the system of equations is a set of nonlinear overdetermined equations. Least square method with lower and upper bounds on the variables [43,44] was used to solve the above set of equations. The forward kinematics problem is then solved given that the eight attachment points (actuators) on the rails move vertically up and down while the eight cables are being shortened or extended to manipulate and control the end effector. Indeed, the conventional cable driven mechanisms have the actuators fixed on the rails while controlling the cable lengths. The following section describes the equations and algorithm used to solve the forward and inverse kinematics.

4.1 Nonlinear model solver

As mentioned earlier, the reconfigurable eight-cable driven mechanism model results in a nonlinear overdetermined set of equations where the number of unknowns is less than the number of equations [45]. The well-known Levenberg Marquardt least squares method [46] is then used to solve the forward kinematics problem represented as KC (refer to Equation 7) according to the following algorithm:

Algorithm 1 FKP

1: ***Procedure*:** OptimizeCableLengths
2: ***Initialization***: $\vec{q}_{er}$, $\vec{q}_{ac}$, $\vec{q}$, time, counter = 1, tol=tolerance
3: **for** counter = 1, 2,…length (time) **do**
4: **set** upper limit, lower limit
5: **while** (min(||KC||)^2>tol)
6: **solve** KC
7: **end while**
8: **update** $\vec{q}_{ac}$ and **record** $\vec{q}$
9: **end for**

Moreover, in conventional CDPM, the forward kinematics is defined as, input: cables length and the output is the pose of the end effector. However, in our reconfigurable mechanism, the forward kinematics is defined as, input: cables length and attachment points location (because attachment points are moving vertically) and the output is the pose of the end effector. In order to evaluate Algorithm 1, a first simulation is done by moving both attachment points $\vec{q}_{ac}$ and cables length ρ_i as an input and $\vec{q}_{er}$ as an output. In order for the reader to be able to replicate the results, parametric equations that describes the linear displacement ($c_i(t,\vec{q})$) of the eight attachment points (actuators) on the rails as well as the elongation and shortening of the eight cables (ρ_i) are shown below in table 3 with the results shown in Figure 4. All the functions are given in terms of time (t) where time is ranged between 0 and 20 seconds in all the simulation results presented in this paper.

i	Attachment points displacement ($c_i(t,\vec{q})$)	Cables length (ρ_i)
1	7.5+0.5×sin(t)	$((3\times(3.25)^2))^{0.5}$-0.5×sin(t)
2	0.5+0.5×sin(t)	$((3\times(3.25)^2))^{0.5}$-0.5×sin(t)
3	7.5+0.5×sin(t)	$((3\times(3.25)^2))^{0.5}$-0.5×sin(t)
4	0.5+0.5×sin(t)	$((3\times(3.25)^2))^{0.5}$-0.5×sin(t)
5	7.5-0.5×sin(t)	$((3\times(3.25)^2))^{0.5}$+0.5×sin(t)
6	0.5-0.5×sin(t)	$((3\times(3.25)^2))^{0.5}$+0.5×sin(t)
7	7.5-0.5×sin(t)	$((3\times(3.25)^2))^{0.5}$+0.5×sin(t)
8	0.5-0.5×sin(t)	$((3\times(3.25)^2))^{0.5}$+0.5×sin(t)

Table 3. Parametric equations of the actuators displacement and the change in cables length (meters)

Figure 4 shows the Cartesian coordinates of the center of mass of the end effector given the position of the eight attachment points on the rails and the eight cable lengths.

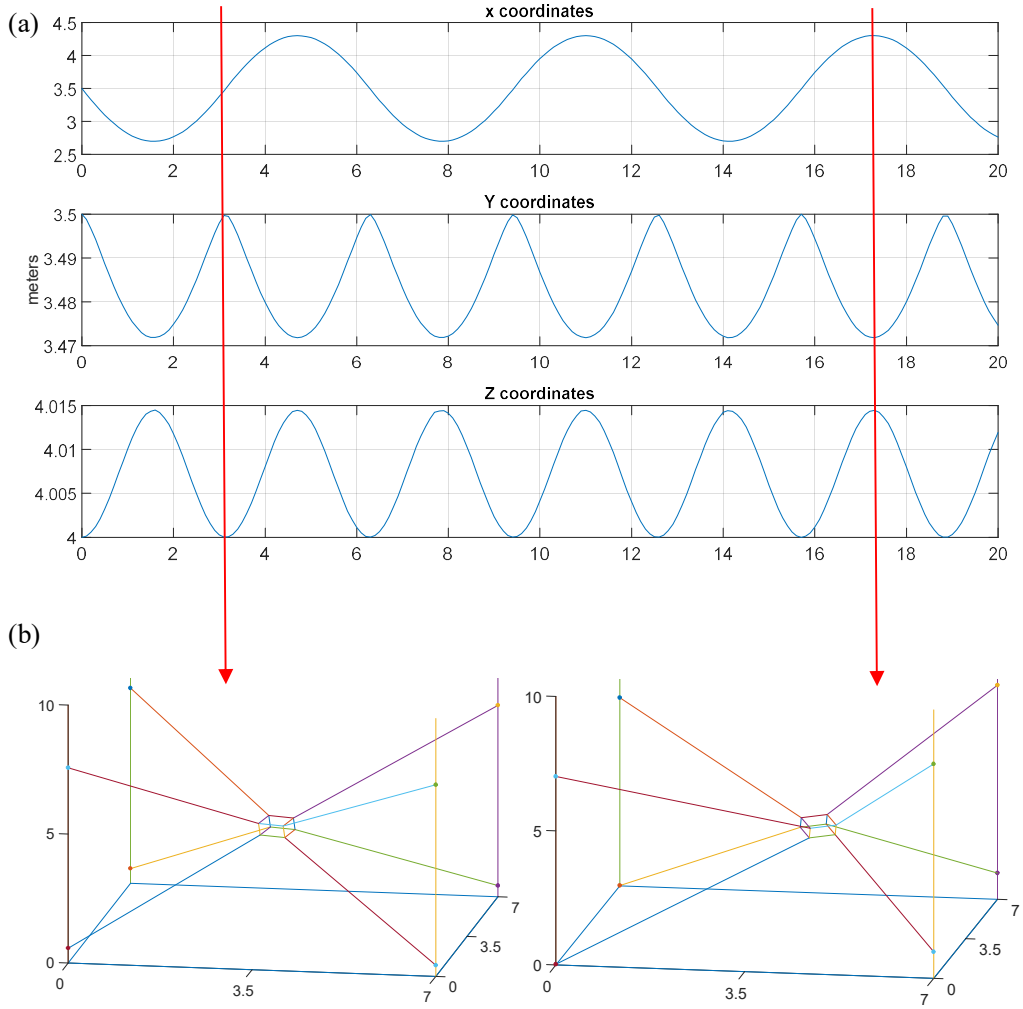

Figure 4(a). X, Y and Z coordinates of the mobile platform center of mass; (b) two pose of the end effector used in the simulation

The inverse kinematic issue is solved; the pose (position and orientation) of the end effector is known in this case as well as the position of the attachment points on the rails, and the unknowns are the eight cables length. Regarding Figure 1, the vector loop-closure equation for cable i is obtained as follows:

$$\rho_i = \left\| \vec{\boldsymbol{r}}_{ef} + \boldsymbol{R}\vec{\boldsymbol{r}}'_i - \vec{\boldsymbol{r}}_{Ai} \right\|, \quad \text{for } i = 1 \text{ to } n \tag{8}$$

Linear programming optimization tool in MATLAB was used to solve Equation 8 for each pose of the end effector. The proposed algorithm can be used also to determine the required positions of the attachment points on the rails given the eight cable lengths. Figure 5 shows the required cable lengths given the full configuration of the end effector (position and orientation) and the position of the attachment points.

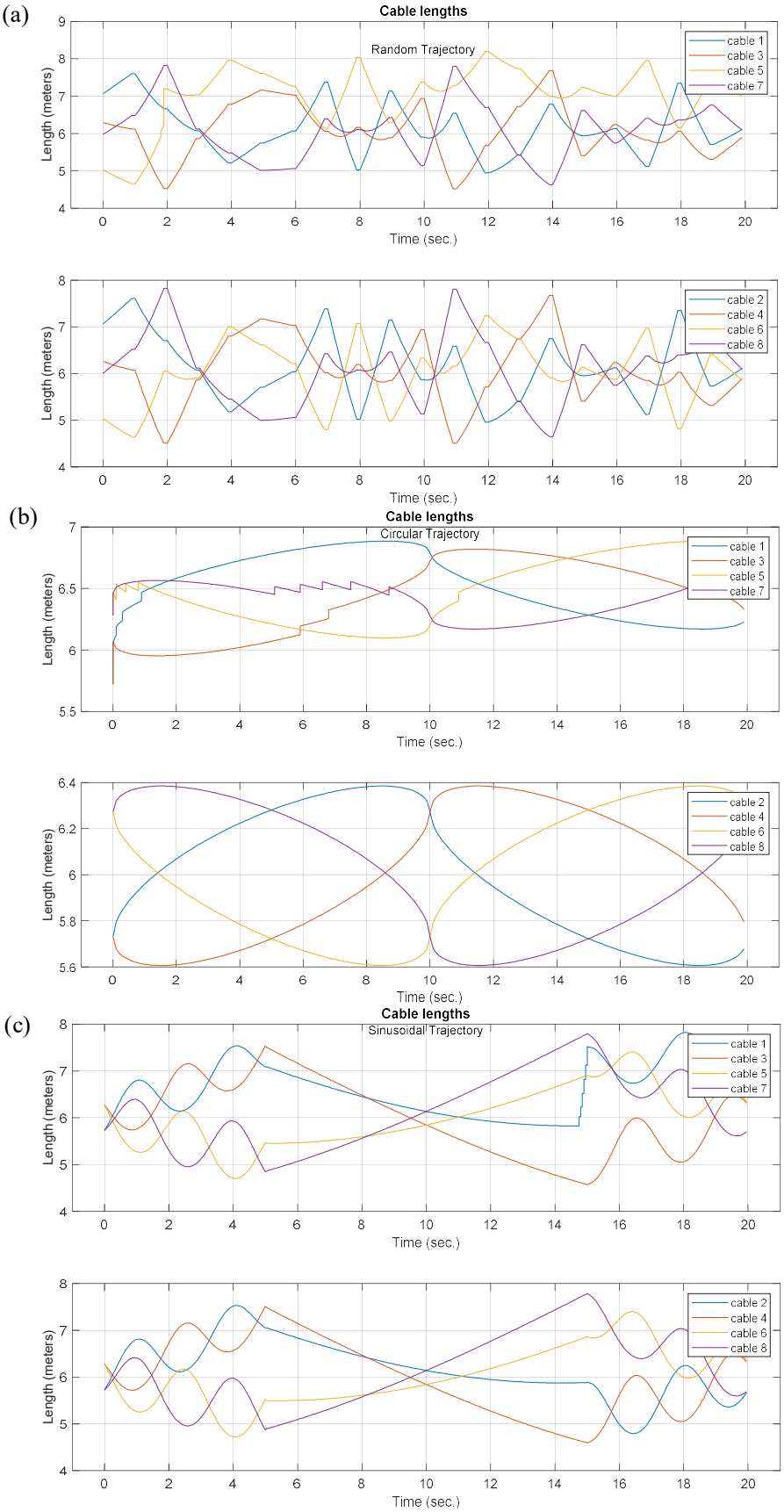

Figure 5. Cables length: a) Random trajectory, (b) Circular trajectory and (c) Sinusoidal trajectory

5 Collision detection calculation

In our study, after solving the forward and inverse kinematics given that the attachment points on the rails move vertically, the reconfiguration idea is then used to solve the collision between cables while maintaining the end effector trajectory by relocating the attachment points on the fixed frame. The online reconfiguration will definitely change the workspace (wrench and feasible) of the mechanism; hence, Section 6.2 shows the difference between initial and final workspace due to the relocation of the attachment points. A cable-cable collision can be treated as two-line interference in 3D, where a collision is detected when these two lines get close to each other to a certain threshold value. In this paper, the cables will be assumed to be massless and straight lines (without sagging), and collision between cables can be geometrically computed as discussed in [47]:
Lines 1 and 2 in Figure 6 can be expressed in 3D in terms of the coordinates of points Q_1, P_1, Q_2 and P_2. One can say that there are two points on line 1 and 2 such that the line connecting these two points is the shortest distance between line 1 and 2. Let's express line 1 and 2 as follows:

$$\begin{Bmatrix} \vec{\boldsymbol{L}}_1 = \vec{\boldsymbol{r}}_{P1} + w\vec{\boldsymbol{d}}_1 \\ \vec{\boldsymbol{L}}_2 = \vec{\boldsymbol{r}}_{P2} + s\vec{\boldsymbol{d}}_2 \end{Bmatrix}, \text{ where } \begin{Bmatrix} \vec{\boldsymbol{d}}_1 = \vec{\boldsymbol{r}}_{Q1} - \vec{\boldsymbol{r}}_{P1} \\ \vec{\boldsymbol{d}}_2 = \vec{\boldsymbol{r}}_{Q2} - \vec{\boldsymbol{r}}_{P2} \end{Bmatrix} \tag{9}$$

where $\vec{\boldsymbol{r}}_{P1}, \vec{\boldsymbol{r}}_{P2}, \vec{\boldsymbol{r}}_{Q1}$ and $\vec{\boldsymbol{r}}_{Q2}$ are the position vectors of P_1, P_2, Q_1 and Q_2 respectively.

w and s are two unique values if and only if lines 1 and 2 are not parallel. By finding w and s, we can define vector $\vec{\mathbf{v}}(w, s)$, whose length is the intended shortest distance between lines 1 and 2. In order to find the two values, w and s, corresponding to the shortest length between lines 1 and 2, it should be realized that $\vec{\mathbf{v}}(w, s)$ in this particular case is perpendicular to the two lines.

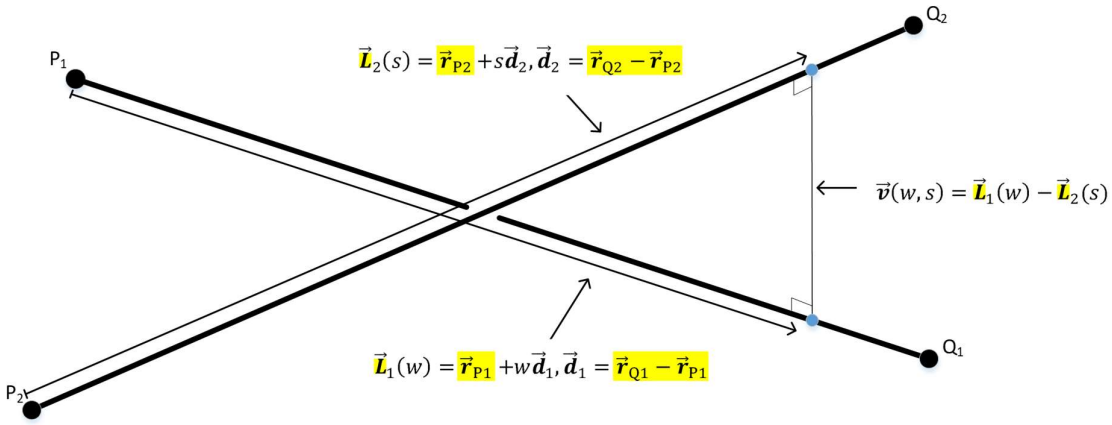

Figure 6. Vector $\vec{\boldsymbol{v}}(\boldsymbol{w}, \boldsymbol{s})$ connecting the two closest points of two lines $\vec{\mathbf{L}}_1$ **and** $\vec{\mathbf{L}}_2$[47]

The perpendicularity conditions can be expressed mathematically as follows:

$$\begin{Bmatrix} \vec{\boldsymbol{d}}_1 \cdot \vec{\boldsymbol{v}}(w,s) = 0 \\ \vec{\boldsymbol{d}}_2 \cdot \vec{\boldsymbol{v}}(w,s) = 0 \end{Bmatrix} \tag{10}$$

Therefore,

$$\begin{Bmatrix} \vec{\boldsymbol{d}}_1 \cdot \left(\vec{\boldsymbol{L}}_1(w) - \vec{\boldsymbol{L}}_2(s)\right) = \vec{\boldsymbol{d}}_1 \cdot \left((\vec{\boldsymbol{r}}_{P1} - \vec{\boldsymbol{r}}_{P2}) + w\vec{\boldsymbol{d}}_1 - s\vec{\boldsymbol{d}}_2\right) = 0 \\ \vec{\boldsymbol{d}}_2 \cdot \left(\vec{\boldsymbol{L}}_1(w) - \vec{\boldsymbol{L}}_2(s)\right) = \vec{\boldsymbol{d}}_2 \cdot \left((\vec{\boldsymbol{r}}_{P1} - \vec{\boldsymbol{r}}_{P2}) + w\vec{\boldsymbol{d}}_1 - s\vec{\boldsymbol{d}}_2\right) = 0 \end{Bmatrix} \tag{11}$$

Rearranging the above equations, s and w may be determined as follows:

$$\begin{Bmatrix} s = (bf - ce)/d \\ w = (af - bc)/d \end{Bmatrix}, \tag{12}$$

where $a = \vec{\boldsymbol{d}}_1.\vec{\boldsymbol{d}}_1, b = \vec{\boldsymbol{d}}_1.\vec{\boldsymbol{d}}_2, c = \vec{\boldsymbol{d}}_1.\vec{\boldsymbol{r}}, e = \vec{\boldsymbol{d}}_2.\vec{\boldsymbol{d}}_2, f = \vec{\boldsymbol{d}}_2.\vec{\boldsymbol{r}}$, $\vec{\boldsymbol{r}} = \vec{\boldsymbol{r}}_{P1} - \vec{\boldsymbol{r}}_{P2}$ and $d = ae - b^2$.

After obtaining s and w, $\vec{\boldsymbol{L}}_1(w)$ and $\vec{\boldsymbol{L}}_2(s)$ can then be computed as well as the coordinates of the two points

connecting the shortest distance ($\vec{\boldsymbol{v}}(w,s)$). The shortest distance between any two cables can then be determined, which is the length of the vector $\vec{\boldsymbol{v}}(w,s)$; hence, it is compared with a threshold value such that the shortest distance value is increased by relocating vertically up and down the corresponding attachment point until the shortest distance between cables exceeds the threshold value, which means that the collision has been avoided, as will be discussed in later sections.

5.1 Cables tension distribution

In this section, the kinematic equations required to solve for tension in the eight cables of the CDPM are established to ensure positive tension among all the cables [48]. Figure 1 shows the schematic for the mobile platform and attachment point A_i, where $\mathscr{R}$ is the fixed global frame, and $\mathscr{E}$ is a local frame attached to the mobile platform.
In case of wrench closure workspace, the cables' tension distribution issue may be expressed as finding all the tensions $\vec{\boldsymbol{t}}_i$ such that:

$$\widetilde{\boldsymbol{w}}\vec{\boldsymbol{t}}_i + \vec{\boldsymbol{w}}_j = \vec{\boldsymbol{0}}_6 \text{ , with } \vec{\boldsymbol{t}}_i > 0, \text{ for } i = 1 \text{ to } n. \tag{13}$$

where,

$\widetilde{\boldsymbol{w}} = \begin{bmatrix} \vec{\boldsymbol{u}}_1 & \vec{\boldsymbol{u}}_2 & \cdots & \vec{\boldsymbol{u}}_8 \\ \vec{\boldsymbol{r}}_1\vec{\boldsymbol{u}}_1 & \vec{\boldsymbol{r}}_2\vec{\boldsymbol{u}}_2 & \cdots & \vec{\boldsymbol{r}}_8\vec{\boldsymbol{u}}_8 \end{bmatrix}_{6\times n}$: Structure matrix,

$\vec{\boldsymbol{t}}_i = \begin{bmatrix} t_1 \\ \vdots \\ t_8 \end{bmatrix}_{n\times 1}$: Cables tension,

$\vec{\boldsymbol{w}}_j = \begin{bmatrix} f_x \\ f_y \\ f_z \\ m_x \\ m_y \\ m_z \end{bmatrix}_{6\times 1}$: External wrench acting on the end effector,

$\vec{\boldsymbol{0}}_6 = \begin{bmatrix} 0 \\ \vdots \\ 0 \end{bmatrix}_{6\times 1}$: Zero vector.

where f_x, f_y, f_z, m_x, m_y and m_z are the components of the external force and moment acting in the X, Y and Z directions respectively. The two variables ($\vec{\boldsymbol{r}}_i$ and $\vec{\boldsymbol{u}}_i$) in the structure matrix $\widetilde{\boldsymbol{w}}$ are explicit functions in the mobile platform position and orientation as well as the attachments points position. These two variables can be computed as follows:

$$\vec{\boldsymbol{u}}_i = \frac{\vec{\boldsymbol{r}}_{ef} + \boldsymbol{R}\vec{\boldsymbol{r}}'_i - \vec{\boldsymbol{r}}_{A_i}}{\left\|\vec{\boldsymbol{r}}_{ef} + \boldsymbol{R}\vec{\boldsymbol{r}}'_i - \vec{\boldsymbol{r}}_{A_i}\right\|} \tag{14}$$

$$\vec{\boldsymbol{r}}_i = \boldsymbol{R}\vec{\boldsymbol{r}}'_i \tag{15}$$

In this study, the wrench feasible condition is applied and an extra condition is added to bind the tension values in the eight cables as follows:

$$t_{min.} < \vec{\boldsymbol{t}}_i < t_{max.}, \tag{16}$$

where $t_{min.}$ is the minimum allowable tension value to ensure that all the cables are taut, and $t_{max.}$ is the maximum allowable tension value depending on the actuators torque.
The feasible closure workspace was solved for all three trajectories given that the only external wrench acting on the end effector is its weight, 25 N, and the maximum and minimum allowable tension values for all the cables are 20 and 120 N respectively. The initial attachment points' (A_i) locations on the rails for the eight cables are shown in Table 4 with respect to the global frame $\mathscr{R}$.

	A_1	A_2	A_3	A_4	A_5	A_6	A_7	A_8
X	0	0	0	0	7	7	7	7

Y	0	0	7	7	7	7	0	0
Z	7.5	0.5	7.5	0.5	7.5	0.5	7.5	0.5

Table 4. Initial positions of the eight attachment points (meters)

Cable tension distribution values are computed using linear programming optimization [42,49,50] to minimize an objective function subjected to equality constraints with lower and upper bounds. Linear programming is chosen since Equation 13 represents linear constraints with no objective function. The results are presented in Figure 7 to guarantee a feasible wrench workspace for three different trajectories. The tension of the eight cables can be observed as positive values (over the zero limit), where the tension values lies between approximate minimum and maximum values, T_{min} = 20 and T_{max} = 90 N.

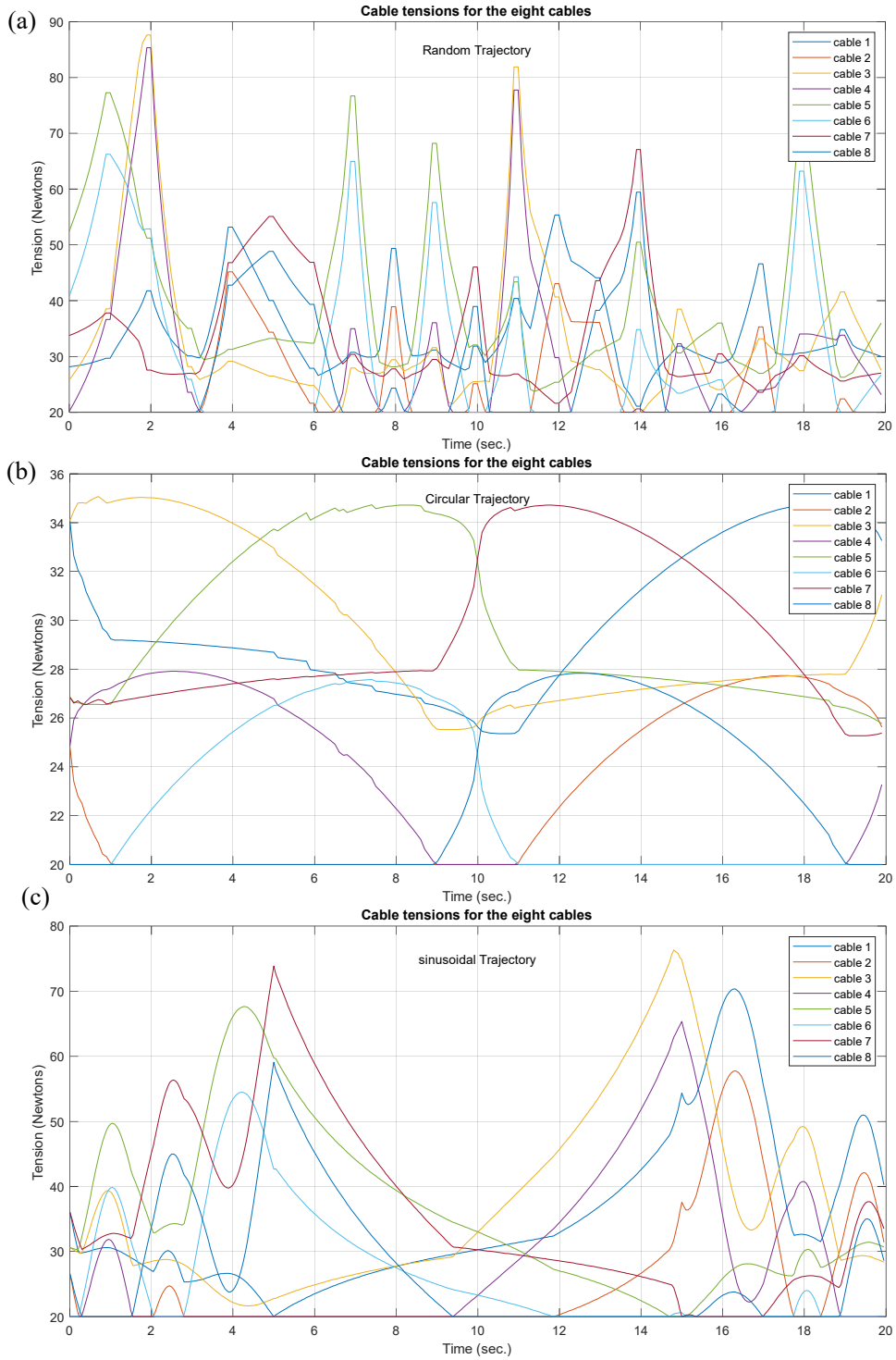

Figure 7. Computed cable tension for the eight cables (Newtons): (a) Random trajectory, (b) Circular trajectory and (c) Sinusoidal trajectory

6 Cable interference avoidance with online reconfiguration

6.1 Cable interference avoidance

The key contribution of this study is the use of online reconfiguration by changing the location of the attachment points of the cables on the fixed rails to avoid a near collision between two cables. A Matlab code was generated

to use the idea of reconfiguration in detecting and eliminating cable-cable interference in real time, as shown the algorithm presented in Figure 8.

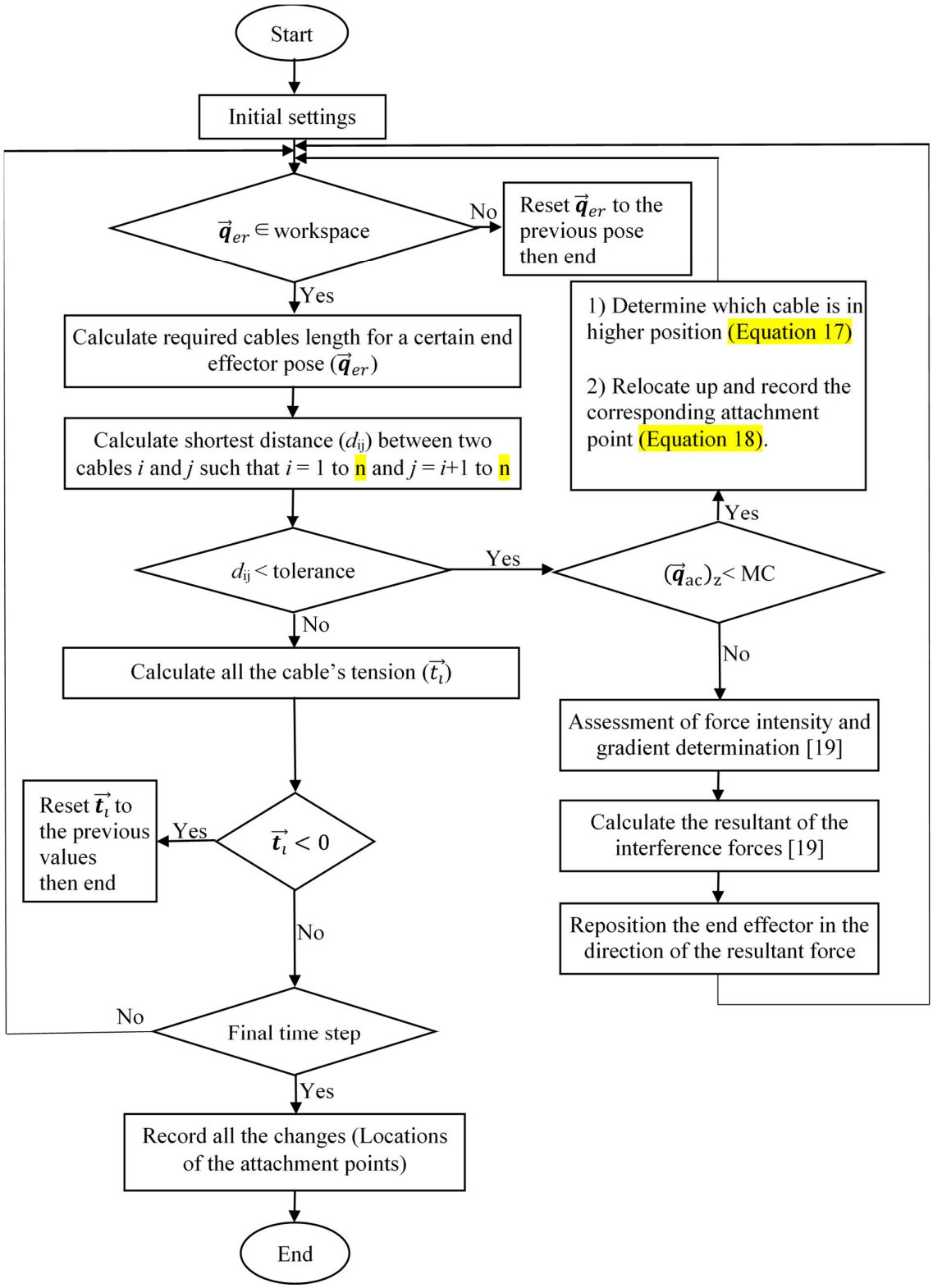

Figure 8. Real time algorithm for detecting and eliminating cable interference

At each time step, the proposed algorithm computes the shortest physical distance (d_{ij}) between all the cables such that i = 1 to n and $j = i$+1 to n and compares it with a threshold value (tolerance) that is defined by the user. The shortest distance calculation depends on the position of the attachment points of the cables on the fixed rails, the pose of the mobile platform and the location of the anchor points on the end effector. In case of a near collision between any two cables, the algorithm computes $\vec{L}_1(w)$ and $\vec{L}_2(s)$ (as shown in Figure 6) and recognizes the coordinates of the two points connecting the shortest distance ($\vec{\mathbf{v}}(w, s)$) and accordingly determines which cable is currently in a higher position as follows:

$$\left\{\begin{array}{c}\text{if } ((\vec{q}_{\text{ac}})_z)_i \geq ((\vec{q}_{\text{ac}})_z)_j \rightarrow \text{then } ((\vec{q}_{\text{ac}})_z)_i \text{ is relocated} \\ \text{Otherwise} \rightarrow ((\vec{q}_{\text{ac}})_z)_j \text{ is relocated}\end{array}\right\} \text{ for } i = 1 \text{ to n.} \quad (17)$$

Hence, it moves up the corresponding attachment point on the rail by a step Δq that is defined by the user. Therefore, the new location of the corresponding attachment point is updated and recorded as follows:

$$(((\vec{q}_{\text{ac}})_z)_{\text{new}})_i = (((\vec{q}_{\text{ac}})_z)_{\text{initial}})_i + \Delta q \text{ for } i = 1 \text{ to n.} \quad (18)$$

In this research study, the step Δq is set to be equal to 0.1 meters, which is approximately 1.5% of the vertical distance between two attachment points on the same rail; however, it can be changed by the user according to the dimension of the mechanism.

It is important to mention here that the location of the reel is moved using a servo linear actuator. The computed location is a set point to the servo controller included in the linear actuator. The servo controller will move the location at its current dynamic like a Heaviside input (step response). This dynamic of the linear actuator is a second order system with damping fixed at 0.7 (compromise between overshoot and settling time). Another solution could be to use a fifth order polynomial trajectory (or a trapezoidal function). However, this will not improve the settling time since the limit is defined by the actuator dynamic. In addition, the robustness of the proposed approach is validated by adding a mechanical limit (MC), as shown in Figure 8, wherein each cable has a maximum vertical location on the rail. MC is defined by the user, and it describes a position on the rail (in meters) that an attachment point cannot exceed. In a case of near collision between two cables where the intended attachment point has already reached its MC, approach suggested by Meziane et al. is adopted [19] since it will be impossible to continue the initial trajectory of the end effector while avoiding cable interference. In the aforementioned method, a repulsive force is generated by a controller, which is computed from the gradient of the shortest distance between the two cables. This repulsive force will act on the end effector in a direction such that the distance between the two cables will be increased.

In order to verify the proposed approach, a simulation was conducted using the above algorithm for three different trajectories. Figure 9 shows the computed distance between cables 1 and 2 as well as the location of the displaced attachment point and its computed tension values for a circular trajectory of the end effector. With the minimum allowable distance (tolerance) between any two cables equal to 0.132 m during the entire time steps and due to the chosen path of the end effector, an interference between pairs of cables is detected within the trajectory of the mobile platform at different times.

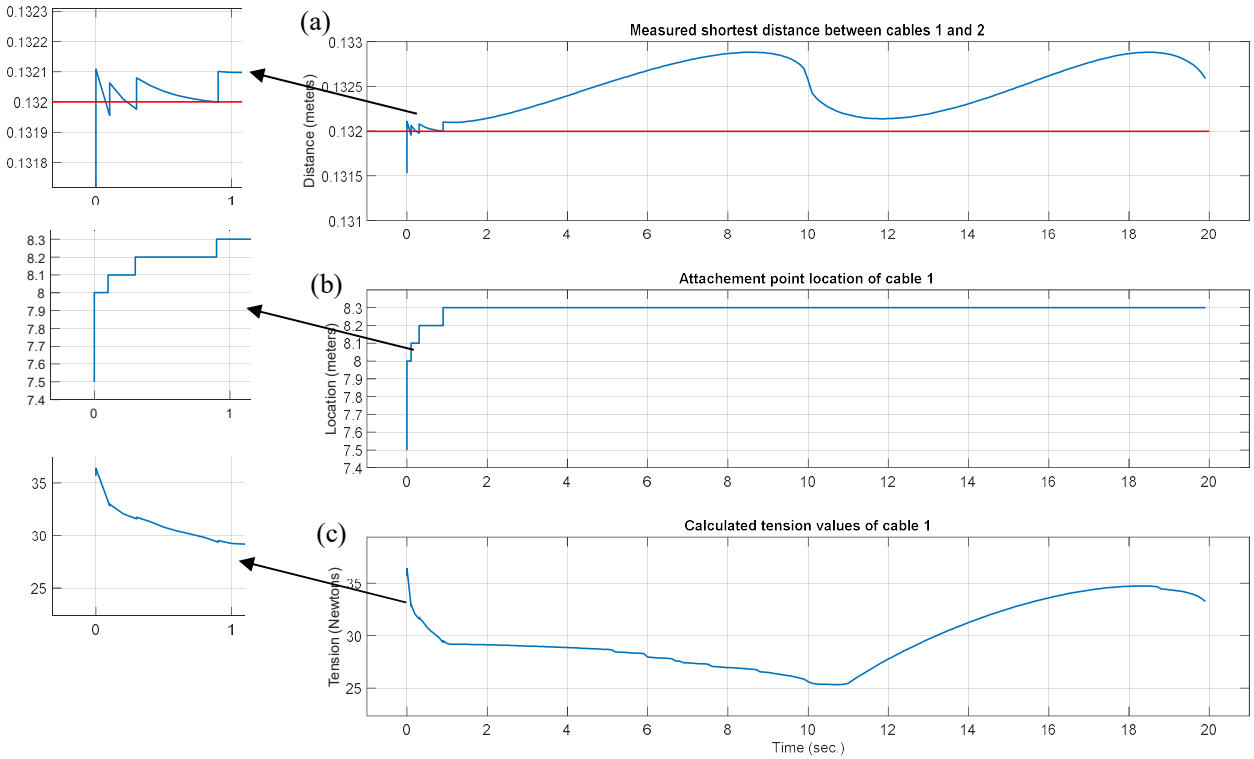

Figure 9. Circular trajectory: (a) measured distance between cables 1 and 2; (b) attachment point location of cable 1; (c) computed tension of cable 1

As shown in Figure 9, at t=0 s, the algorithm detects the shortest distance between cables 1 and 2 below the threshold value (0.132 m – horizontal line in red). Also, it determines that cable 1 is in a higher position; hence, the attachment point of cable 1 which was initially at location 7.5 m, measured from the ground, starts to increase with an increment of 0.1 m. It keeps increasing while the distance is being measured until the distance between the two cables reaches more than 0.132 m and the attachment point location reaches 8.3 m at t=0.9 s. After that, the measured shortest distance between the two cables is above the threshold value.

The measured shortest distance between cables 1 and 2 and the attachment points locations of cable 1 are shown in Figure 10 for a sinusoidal trajectory of the end effector, and the minimum allowable distance between cables equals to 0.118 m.

.

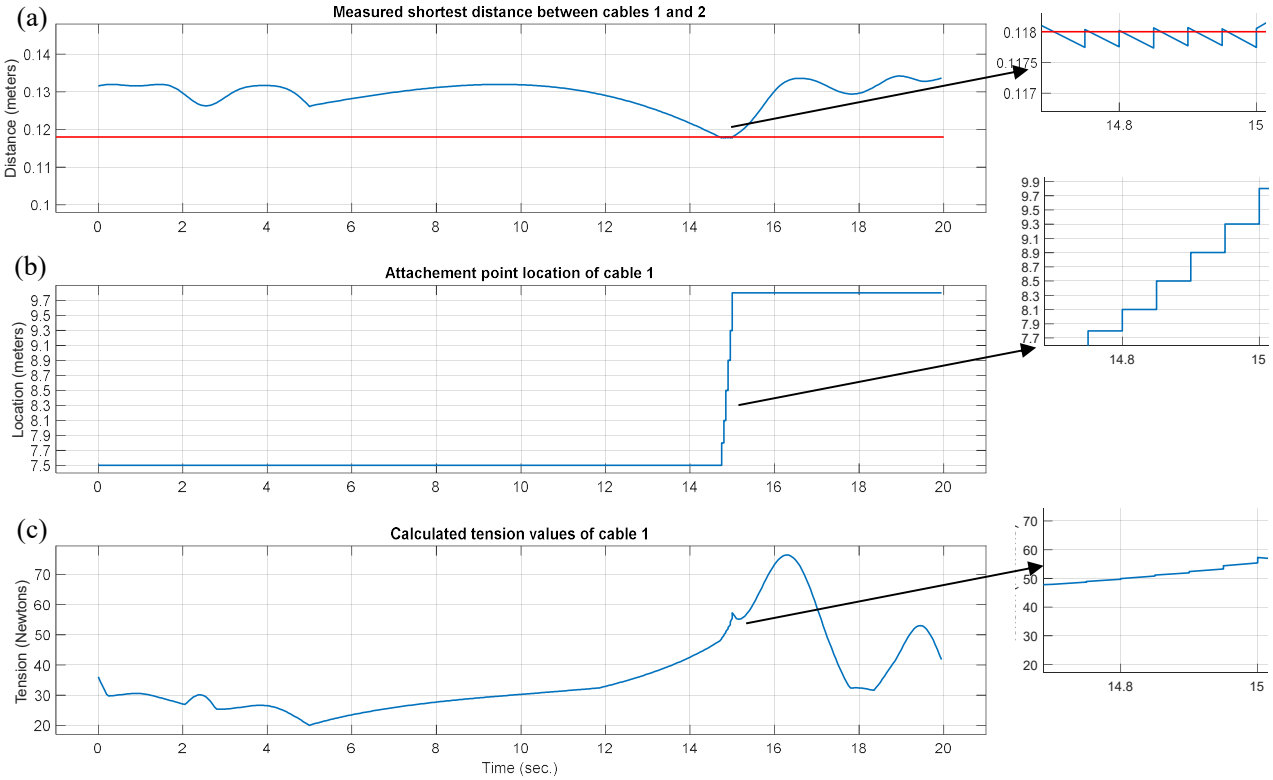

Figure 10. Sinusoidal trajectory: (a) measured distance between cables 1 and 2; (b) attachment points locations of cable 1; (c) computed tension of cable 1

At t=14.75 s, the algorithm detects a shortest distance below the threshold value. It also determines that cable 1 is in a higher position. Accordingly, the attachment point location of cable 1 starts to rise, causing an increase in the perpendicular distance between the two cables to avoid collision. The measured distance between the two cables is detected to keep falling below the threshold value until t=15 s (Figure 10 (a) - enlarged image) due to the end effector trajectory. Accordingly, the algorithm kept moving up the attachment point of the higher cable, which is cable 1, in order to prevent interference until it reached 9.8 m.

Figure 11 shows the computed distance between cables 5 and 6 as well as the corresponding attachment points locations for a random trajectory of the end effector with the minimum allowable distance (tolerance) between any two cables equal to 0.119 m. The random trajectory in Cartesian coordinates was generated by MATLAB; however, as mentioned earlier, the trajectory data are available in appendix A in order to allow the reader to be able to replicate the results.

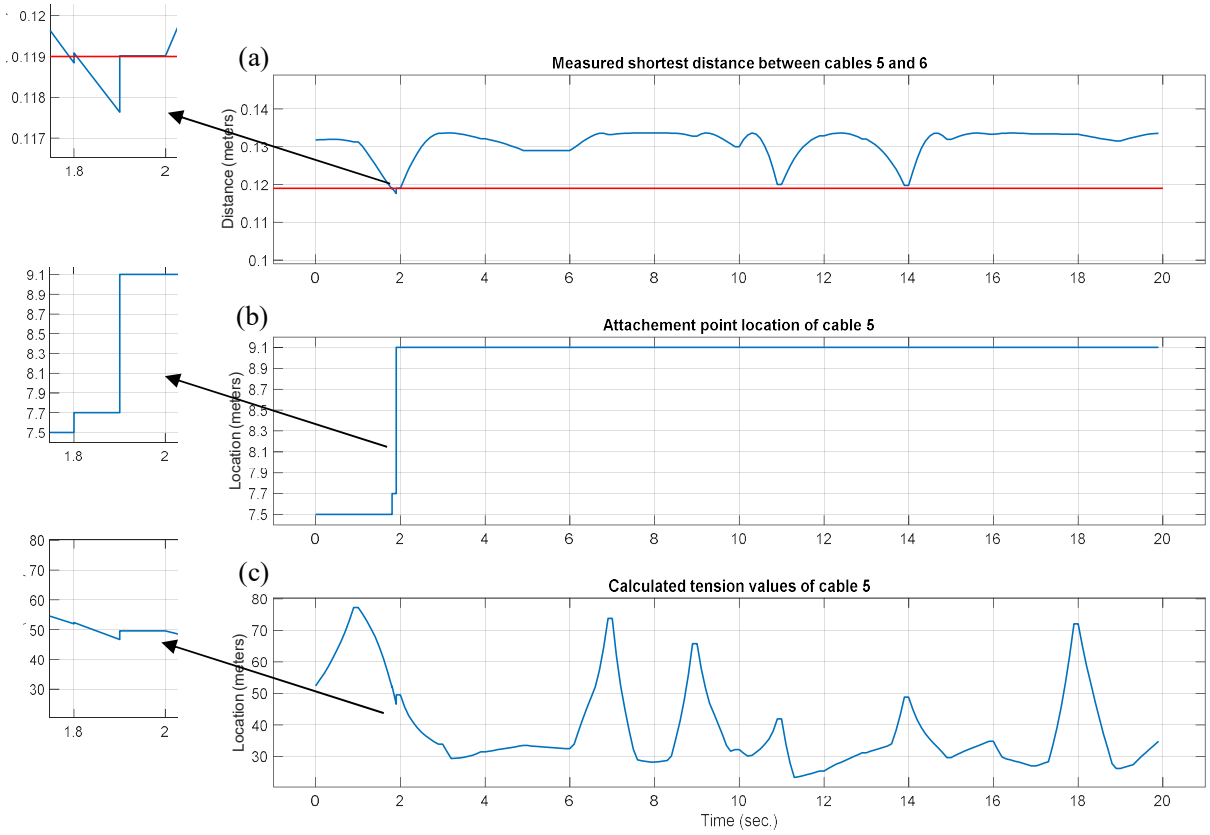

Figure 11. Random trajectory: (a) measured distance between cables 5 and 6; (b) attachment points locations of cable 5; (c) computed tension of cable 5

As shown in Figure 11, at t=1.8 s, the algorithm detects the first shortest distance between cables 5 and 6 below 0.119 m. Also, it determines that cable 5 is in a higher position than cable 6; hence, the attachment point of cable 5, which was initially at location 7.5 m, measured from the ground, started to increase with an increment of 0.1 m. It keeps increasing while the distance is measured until the distance between the two cables reaches more than 0.119 m and the attachment point location reaches 9.1 m at t=1.9 s. After that, the measured shortest distance between the two cables is the threshold value.

6.2 Effect on the wrench feasible workspace

The wrench feasible workspace of cable driven parallel mechanisms is defined as all the set of poses of the end effector such that all the cables remain taut (positive tension) within specific upper and lower values while balancing an external wrench (forces and/or moments) acting on the mobile platform [51]. In this study, the feasible workspace is mapped by satisfying equations 13 and 16 by testing a 3D grid of points lying within the physical limits of the mechanism. With respect to Equation 13, the external wrench in this study is set to 25 N acting in the negative Z direction, which represents the weight of the mobile platform. In addition, the allowed upper and lower tensions induced within the eight cables were set to 120 N and 20 N respectively. It is also possible to set specific upper and/or lower values for each cable separately. The feasible workspace was mapped for every change occurring in any of the attachment points on the rails; however, the initial and final workspaces are shown in this study for the sake of comparison.

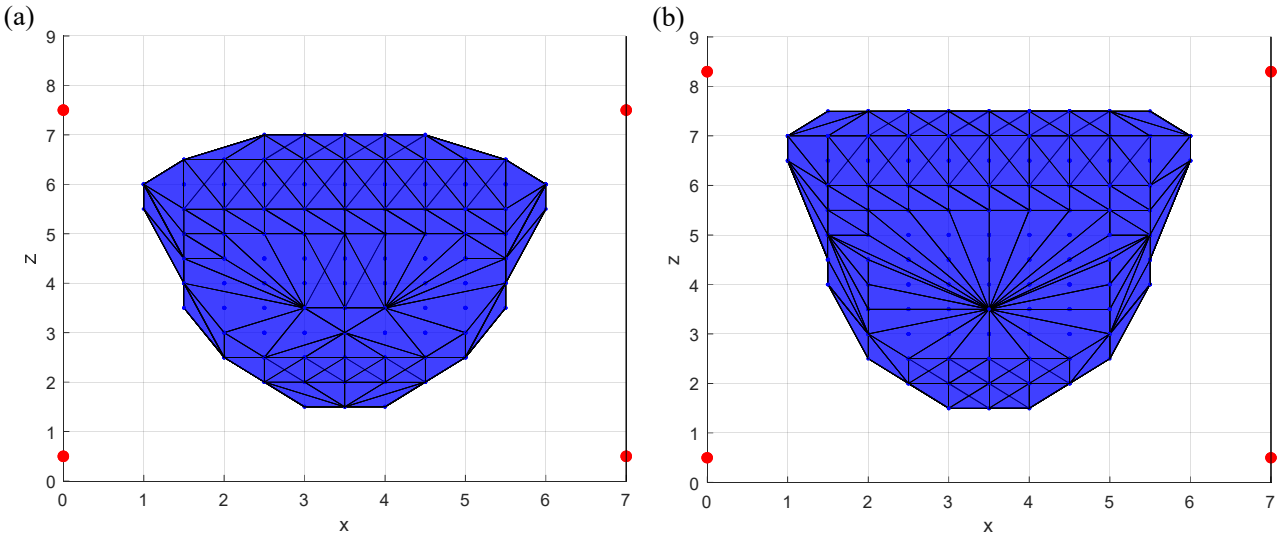

Figure 12. Circular trajectory: (a) initial workspace and (b) final workspace

It is observed in Figure 12 that the workspace increased from an upper limit of 7 m (Figure 12 (a)) to 7.5 m (Figure 12 (b)). This change was a direct result of the change in the four upper attachment points' locations (red points), which were initially at a distance 7.5 m from the ground but increased to 8.3 m to avoid collision with other cables during the circular trajectory of the end effector as discussed in Section 6.1.

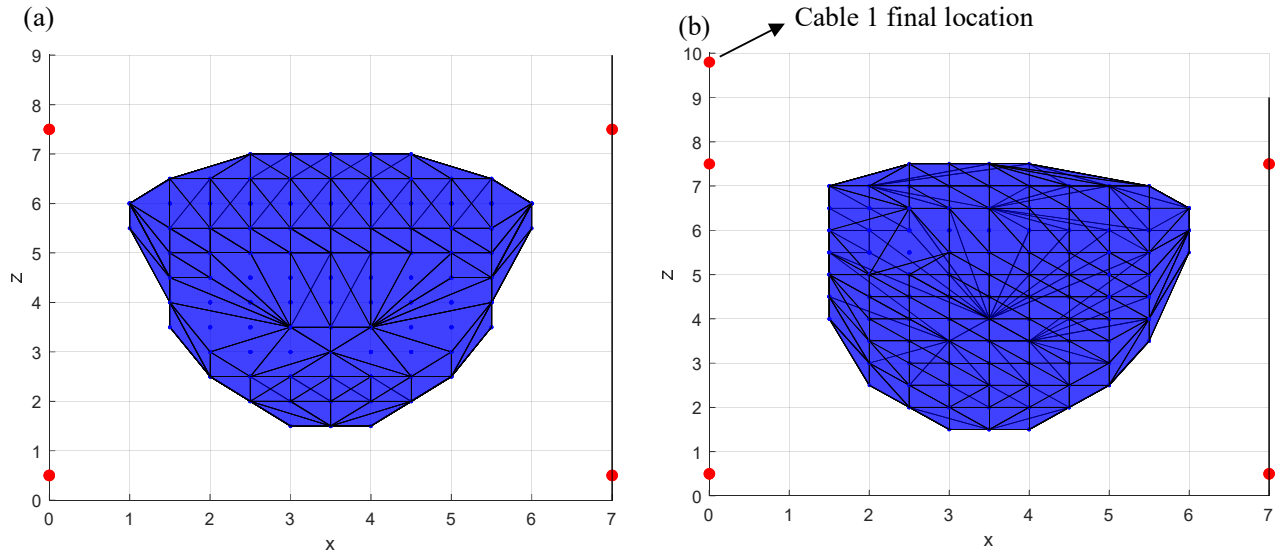

Figure 13. Sinusoidal trajectory (a) initial workspace and (b) final workspace

Figure 13 shows the initial and final feasible workspaces due to the change in the location of cable 1 from 7.5 m (Figure 13 (a)) to 9.8 m (Figure 13 (b)). As shown, the workspace increased in the z direction from an upper limit of 7 m to a limit of 7.5 m due to the change in one attachment point location, which is that of cable 1. It was also noted that the shape of the left side of the workspace changed from an inclined surface to a flat surface, and the limit decreased by almost 0.5 m.

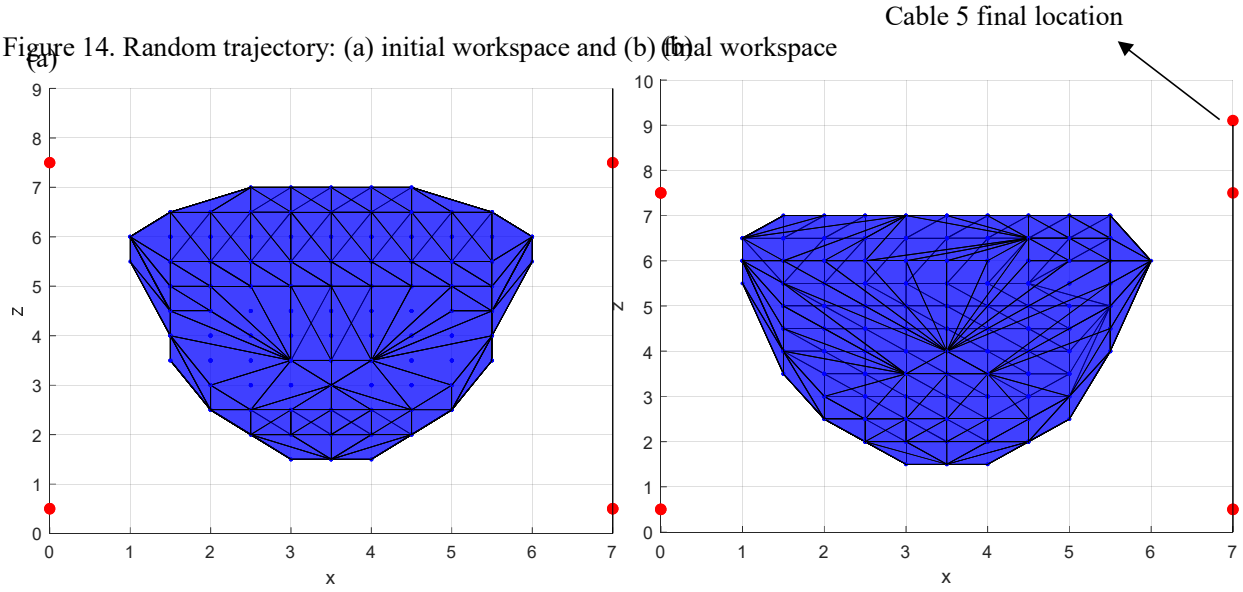

Figure 14. Random trajectory: (a) initial workspace and (b) final workspace

Figure 14 shows the initial and final feasible workspaces due to the change in the location of cable 5 from 7.5 m to 9.1 m. It was noted that there was no significant change in the workspace limit; however, the workspace shape changed from inclined corners on the top (Figure 14 (a)) to a flat surface (Figure 14 (b)). Also, the right and left sides of the workspace volume slightly increased when both figures are compared.

7 Conclusion

The main contributions of this study include the following: First, to model a reconfigurable fully constrained cable driven parallel mechanism with moving base attachment points using non-linear multibody dynamics approach. Using this model, the forward kinematics issue is solved given that the eight attachment points move vertically on the rails, while the eight cables control the end effector. In addition, the inverse kinematics issue is solved by determining the required lengths of the eight cables given the pose of the end-effector and the positions of the eight movable attachment points on the rails. The second contribution is that the reconfigurable idea is used to avoid interference between cables while maintaining the trajectory of the mobile platform. An algorithm was created in order to detect a near collision between any two cables and determine which cable is in a higher position; hence, it moves up the corresponding attachment point to increase the shortest distance between the two cables until it reaches a safe threshold value. The new approach was tested by creating three different simulated trajectories with intended cable interference. As shown in the results, during a specific trajectory for the mobile platform, the algorithm effectively detected a near collision between cables 1 and 2 in the first two trajectories and between cables 5 and 6 in the last trajectory. Accordingly, the corresponding attachment points of the upper cables moved up to increase the distance between the two cables and avoid collision. The reconfiguration idea is used based on relocation of the attachment points on the rails unlike conventional cable driven mechanisms where the attachment points are fixed on the rails. As a consequence of relocating the attachment points on the fixed frame, the wrench feasible workspace mapping was obtained, and the influence of real time reconfiguration on feasible workspaces is presented. It was shown that the change in attachment point location increased and changed the shape of the workspace volume, as discussed in Section 6.2.

Funding

This work received financial support from the Fonds de recherche du Québec—Nature et technologies (FRQNT), under grant number 2016-PR-188869, and the FRQ-NT strategic network REPARTI.

Appendix A

For all the trajectories, the height of the end effector's center of mass is 4 m and the three orientation angles are zero.

Circular trajectory:

time	X	Y	time	X	Y	time	X	Y	time	X	Y	time	X	Y
0.1	3	3.5	4.1	3.4	3.99	8.1	3.8	3.9	12.1	3.8	3.1	16.1	3.4	3.01
0.2	3.01	3.599	4.2	3.41	3.992	8.2	3.81	3.892	12.2	3.79	3.093	16.2	3.39	3.012
0.3	3.02	3.64	4.3	3.42	3.994	8.3	3.82	3.884	12.3	3.78	3.086	16.3	3.38	3.015
0.4	3.03	3.671	4.4	3.43	3.995	8.4	3.83	3.876	12.4	3.77	3.079	16.4	3.37	3.017
0.5	3.04	3.696	4.5	3.44	3.996	8.5	3.84	3.867	12.5	3.76	3.073	16.5	3.36	3.02
0.6	3.05	3.718	4.6	3.45	3.997	8.6	3.85	3.857	12.6	3.75	3.067	16.6	3.35	3.023
0.7	3.06	3.737	4.7	3.46	3.998	8.7	3.86	3.847	12.7	3.74	3.061	16.7	3.34	3.026
0.8	3.07	3.755	4.8	3.47	3.999	8.8	3.87	3.836	12.8	3.73	3.056	16.8	3.33	3.03
0.9	3.08	3.771	4.9	3.48	4	8.9	3.88	3.825	12.9	3.72	3.051	16.9	3.32	3.034
1	3.09	3.786	5	3.49	4	9	3.89	3.813	13	3.71	3.046	17	3.31	3.038
1.1	3.1	3.8	5.1	3.5	4	9.1	3.9	3.8	13.1	3.7	3.042	17.1	3.3	3.042
1.2	3.11	3.813	5.2	3.51	4	9.2	3.91	3.786	13.2	3.69	3.038	17.2	3.29	3.046
1.3	3.12	3.825	5.3	3.52	4	9.3	3.92	3.771	13.3	3.68	3.034	17.3	3.28	3.051
1.4	3.13	3.836	5.4	3.53	3.999	9.4	3.93	3.755	13.4	3.67	3.03	17.4	3.27	3.056
1.5	3.14	3.847	5.5	3.54	3.998	9.5	3.94	3.737	13.5	3.66	3.026	17.5	3.26	3.061
1.6	3.15	3.857	5.6	3.55	3.997	9.6	3.95	3.718	13.6	3.65	3.023	17.6	3.25	3.067
1.7	3.16	3.867	5.7	3.56	3.996	9.7	3.96	3.696	13.7	3.64	3.02	17.7	3.24	3.073
1.8	3.17	3.876	5.8	3.57	3.995	9.8	3.97	3.671	13.8	3.63	3.017	17.8	3.23	3.079
1.9	3.18	3.884	5.9	3.58	3.994	9.9	3.98	3.64	13.9	3.62	3.015	17.9	3.22	3.086
2	3.19	3.892	6	3.59	3.992	10	3.99	3.599	14	3.61	3.012	18	3.21	3.093
2.1	3.2	3.9	6.1	3.6	3.99	10.1	4	3.5	14.1	3.6	3.01	18.1	3.2	3.1
2.2	3.21	3.907	6.2	3.61	3.988	10.2	3.99	3.401	14.2	3.59	3.008	18.2	3.19	3.108
2.3	3.22	3.914	6.3	3.62	3.985	10.3	3.98	3.36	14.3	3.58	3.006	18.3	3.18	3.116
2.4	3.23	3.921	6.4	3.63	3.983	10.4	3.97	3.329	14.4	3.57	3.005	18.4	3.17	3.124
2.5	3.24	3.927	6.5	3.64	3.98	10.5	3.96	3.304	14.5	3.56	3.004	18.5	3.16	3.133
2.6	3.25	3.933	6.6	3.65	3.977	10.6	3.95	3.282	14.6	3.55	3.003	18.6	3.15	3.143
2.7	3.26	3.939	6.7	3.66	3.974	10.7	3.94	3.263	14.7	3.54	3.002	18.7	3.14	3.153
2.8	3.27	3.944	6.8	3.67	3.97	10.8	3.93	3.245	14.8	3.53	3.001	18.8	3.13	3.164
2.9	3.28	3.949	6.9	3.68	3.966	10.9	3.92	3.229	14.9	3.52	3	18.9	3.12	3.175
3	3.29	3.954	7	3.69	3.962	11	3.91	3.214	15	3.51	3	19	3.11	3.187
3.1	3.3	3.958	7.1	3.7	3.958	11.1	3.9	3.2	15.1	3.5	3	19.1	3.1	3.2
3.2	3.31	3.962	7.2	3.71	3.954	11.2	3.89	3.187	15.2	3.49	3	19.2	3.09	3.214
3.3	3.32	3.966	7.3	3.72	3.949	11.3	3.88	3.175	15.3	3.48	3	19.3	3.08	3.229
3.4	3.33	3.97	7.4	3.73	3.944	11.4	3.87	3.164	15.4	3.47	3.001	19.4	3.07	3.245
3.5	3.34	3.974	7.5	3.74	3.939	11.5	3.86	3.153	15.5	3.46	3.002	19.5	3.06	3.263
3.6	3.35	3.977	7.6	3.75	3.933	11.6	3.85	3.143	15.6	3.45	3.003	19.6	3.05	3.282
3.7	3.36	3.98	7.7	3.76	3.927	11.7	3.84	3.133	15.7	3.44	3.004	19.7	3.04	3.304
3.8	3.37	3.983	7.8	3.77	3.921	11.8	3.83	3.124	15.8	3.43	3.005	19.8	3.03	3.329
3.9	3.38	3.985	7.9	3.78	3.914	11.9	3.82	3.116	15.9	3.42	3.006	19.9	3.02	3.36
4	3.39	3.988	8	3.79	3.907	12	3.81	3.108	16	3.41	3.008	20	3.01	3.401

Sinusoidal trajectory:

time	X	Y	time	X	Y	time	X	Y	time	X	Y	time	X	Y
0.1	3.5	3	4.1	5.1	4.5	8.1	4.3	3.47	12.1	2.7	4.06	16.1	1.9	3
0.2	3.54	3.19	4.2	5.14	4.48	8.2	4.26	3.49	12.2	2.66	4.08	16.2	1.94	2.83
0.3	3.58	3.4	4.3	5.18	4.41	8.3	4.22	3.5	12.3	2.62	4.09	16.3	1.98	2.69
0.4	3.62	3.6	4.4	5.22	4.31	8.4	4.18	3.52	12.4	2.58	4.11	16.4	2.02	2.59
0.5	3.66	3.81	4.5	5.26	4.17	8.5	4.14	3.53	12.5	2.54	4.12	16.5	2.06	2.52
0.6	3.7	4	4.6	5.3	4	8.6	4.1	3.55	12.6	2.5	4.14	16.6	2.1	2.5
0.7	3.74	4.17	4.7	5.34	3.81	8.7	4.06	3.56	12.7	2.46	4.15	16.7	2.14	2.52
0.8	3.78	4.31	4.8	5.38	3.6	8.8	4.02	3.58	12.8	2.42	4.17	16.8	2.18	2.59
0.9	3.82	4.41	4.9	5.42	3.4	8.9	3.98	3.59	12.9	2.38	4.18	16.9	2.22	2.69
1	3.86	4.48	5	5.46	3.19	9	3.94	3.6	13	2.34	4.2	17	2.26	2.83
1.1	3.9	4.5	5.1	5.5	3	9.1	3.9	3.62	13.1	2.3	4.21	17.1	2.3	3
1.2	3.94	4.48	5.2	5.46	3.04	9.2	3.86	3.63	13.2	2.26	4.23	17.2	2.34	3.19
1.3	3.98	4.41	5.3	5.42	3.06	9.3	3.82	3.65	13.3	2.22	4.24	17.3	2.38	3.4
1.4	4.02	4.31	5.4	5.38	3.07	9.4	3.78	3.66	13.4	2.18	4.26	17.4	2.42	3.6
1.5	4.06	4.17	5.5	5.34	3.09	9.5	3.74	3.68	13.5	2.14	4.27	17.5	2.46	3.81
1.6	4.1	4	5.6	5.3	3.1	9.6	3.7	3.69	13.6	2.1	4.29	17.6	2.5	4
1.7	4.14	3.81	5.7	5.26	3.12	9.7	3.66	3.71	13.7	2.06	4.3	17.7	2.54	4.17
1.8	4.18	3.6	5.8	5.22	3.13	9.8	3.62	3.72	13.8	2.02	4.32	17.8	2.58	4.31
1.9	4.22	3.4	5.9	5.18	3.15	9.9	3.58	3.74	13.9	1.98	4.33	17.9	2.62	4.41
2	4.26	3.19	6	5.14	3.16	10	3.54	3.75	14	1.94	4.34	18	2.66	4.48
2.1	4.3	3	6.1	5.1	3.18	10.1	3.5	3.77	14.1	1.9	4.36	18.1	2.7	4.5
2.2	4.34	2.83	6.2	5.06	3.19	10.2	3.46	3.78	14.2	1.86	4.37	18.2	2.74	4.48
2.3	4.38	2.69	6.3	5.02	3.21	10.3	3.42	3.8	14.3	1.82	4.39	18.3	2.78	4.41
2.4	4.42	2.59	6.4	4.98	3.22	10.4	3.38	3.81	14.4	1.78	4.4	18.4	2.82	4.31
2.5	4.46	2.52	6.5	4.94	3.23	10.5	3.34	3.83	14.5	1.74	4.42	18.5	2.86	4.17
2.6	4.5	2.5	6.6	4.9	3.25	10.6	3.3	3.84	14.6	1.7	4.43	18.6	2.9	4
2.7	4.54	2.52	6.7	4.86	3.26	10.7	3.26	3.86	14.7	1.66	4.45	18.7	2.94	3.81
2.8	4.58	2.59	6.8	4.82	3.28	10.8	3.22	3.87	14.8	1.62	4.46	18.8	2.98	3.6
2.9	4.62	2.69	6.9	4.78	3.29	10.9	3.18	3.89	14.9	1.58	4.48	18.9	3.02	3.4
3	4.66	2.83	7	4.74	3.31	11	3.14	3.9	15	1.54	4.49	19	3.06	3.19
3.1	4.7	3	7.1	4.7	3.32	11.1	3.1	3.92	15.1	1.5	4.51	19.1	3.1	3
3.2	4.74	3.19	7.2	4.66	3.34	11.2	3.06	3.93	15.2	1.54	4.48	19.2	3.14	2.83
3.3	4.78	3.4	7.3	4.62	3.35	11.3	3.02	3.95	15.3	1.58	4.41	19.3	3.18	2.69
3.4	4.82	3.6	7.4	4.58	3.37	11.4	2.98	3.96	15.4	1.62	4.31	19.4	3.22	2.59
3.5	4.86	3.81	7.5	4.54	3.38	11.5	2.94	3.97	15.5	1.66	4.17	19.5	3.26	2.52
3.6	4.9	4	7.6	4.5	3.4	11.6	2.9	3.99	15.6	1.7	4	19.6	3.3	2.5
3.7	4.94	4.17	7.7	4.46	3.41	11.7	2.86	4	15.7	1.74	3.81	19.7	3.34	2.52
3.8	4.98	4.31	7.8	4.42	3.43	11.8	2.82	4.02	15.8	1.78	3.6	19.8	3.38	2.59
3.9	5.02	4.41	7.9	4.38	3.44	11.9	2.78	4.03	15.9	1.82	3.4	19.9	3.42	2.69
4	5.06	4.48	8	4.34	3.46	12	2.74	4.05	16	1.86	3.19	20	3.46	2.83

Random trajectory:

time	X	Y	time	X	Y	time	X	Y	time	X	Y	time	X	Y
0.1	4.56	4.3	4.1	3.28	2.05	8.1	2.6	2.52	12.1	1.98	2.9	16.1	3.84	3.39
0.2	4.58	4.38	4.2	3.37	2.06	8.2	2.78	2.77	12.2	2.14	2.83	16.2	3.68	3.34
0.3	4.59	4.47	4.3	3.46	2.06	8.3	2.96	3.01	12.3	2.31	2.76	16.3	3.52	3.29
0.4	4.6	4.55	4.4	3.55	2.07	8.4	3.14	3.26	12.4	2.48	2.7	16.4	3.36	3.23
0.5	4.61	4.64	4.5	3.64	2.07	8.5	3.32	3.51	12.5	2.65	2.63	16.5	3.2	3.18
0.6	4.63	4.72	4.6	3.73	2.08	8.6	3.5	3.76	12.6	2.82	2.56	16.6	3.04	3.12
0.7	4.64	4.81	4.7	3.82	2.08	8.7	3.68	4.01	12.7	2.99	2.49	16.7	2.88	3.07
0.8	4.65	4.89	4.8	3.91	2.09	8.8	3.86	4.26	12.8	3.16	2.42	16.8	2.72	3.01
0.9	4.67	4.98	4.9	4	2.09	8.9	4.04	4.51	12.9	3.32	2.35	16.9	2.56	2.96
1	4.68	5.06	5	4.09	2.1	9	4.22	4.76	13	3.49	2.29	17	2.4	2.91
1.1	4.68	5.06	5.1	4.09	2.1	9.1	4.22	4.76	13.1	3.49	2.29	17.1	2.4	2.91
1.2	4.41	5.09	5.2	4.11	2.15	9.2	4.21	4.5	13.2	3.7	2.31	17.2	2.63	3.12
1.3	4.14	5.12	5.3	4.14	2.19	9.3	4.2	4.25	13.3	3.9	2.33	17.3	2.86	3.33
1.4	3.87	5.15	5.4	4.17	2.24	9.4	4.19	4	13.4	4.11	2.36	17.4	3.1	3.55
1.5	3.6	5.19	5.5	4.2	2.29	9.5	4.18	3.74	13.5	4.31	2.38	17.5	3.33	3.76
1.6	3.33	5.22	5.6	4.23	2.34	9.6	4.16	3.49	13.6	4.52	2.41	17.6	3.57	3.97
1.7	3.06	5.25	5.7	4.25	2.39	9.7	4.15	3.24	13.7	4.72	2.43	17.7	3.8	4.18
1.8	2.79	5.28	5.8	4.28	2.43	9.8	4.14	2.98	13.8	4.93	2.46	17.8	4.04	4.4
1.9	2.52	5.31	5.9	4.31	2.48	9.9	4.13	2.73	13.9	5.13	2.48	17.9	4.27	4.61
2	2.25	5.34	6	4.34	2.53	10	4.12	2.47	14	5.34	2.5	18	4.51	4.82
2.1	2.25	5.34	6.1	4.34	2.53	10.1	4.12	2.47	14.1	5.34	2.5	18.1	4.51	4.82
2.2	2.38	5.15	6.2	4.36	2.79	10.2	3.9	2.78	14.2	5.06	2.67	18.2	4.28	4.71
2.3	2.52	4.97	6.3	4.38	3.05	10.3	3.68	3.08	14.3	4.79	2.83	18.3	4.06	4.61
2.4	2.65	4.79	6.4	4.4	3.31	10.4	3.46	3.39	14.4	4.51	2.99	18.4	3.84	4.5
2.5	2.79	4.6	6.5	4.42	3.57	10.5	3.24	3.69	14.5	4.24	3.15	18.5	3.62	4.39
2.6	2.92	4.42	6.6	4.44	3.83	10.6	3.03	4	14.6	3.96	3.32	18.6	3.4	4.28
2.7	3.06	4.24	6.7	4.46	4.09	10.7	2.81	4.3	14.7	3.69	3.48	18.7	3.18	4.17
2.8	3.19	4.06	6.8	4.48	4.34	10.8	2.59	4.61	14.8	3.41	3.64	18.8	2.96	4.06
2.9	3.32	3.87	6.9	4.5	4.6	10.9	2.37	4.91	14.9	3.14	3.8	18.9	2.74	3.95
3	3.46	3.69	7	4.52	4.86	11	2.15	5.22	15	2.86	3.96	19	2.52	3.84
3.1	3.46	3.69	7.1	4.52	4.86	11.1	2.15	5.22	15.1	2.86	3.96	19.1	2.52	3.84
3.2	3.44	3.51	7.2	4.31	4.6	11.2	2.13	4.96	15.2	2.97	3.9	19.2	2.63	3.83
3.3	3.42	3.33	7.3	4.09	4.34	11.3	2.11	4.7	15.3	3.08	3.84	19.3	2.74	3.81
3.4	3.4	3.14	7.4	3.88	4.08	11.4	2.09	4.44	15.4	3.19	3.77	19.4	2.85	3.79
3.5	3.38	2.96	7.5	3.67	3.82	11.5	2.07	4.19	15.5	3.3	3.71	19.5	2.97	3.78
3.6	3.36	2.78	7.6	3.46	3.56	11.6	2.05	3.93	15.6	3.41	3.65	19.6	3.08	3.76
3.7	3.34	2.6	7.7	3.24	3.3	11.7	2.03	3.67	15.7	3.51	3.58	19.7	3.19	3.75
3.8	3.32	2.42	7.8	3.03	3.04	11.8	2.01	3.41	15.8	3.62	3.52	19.8	3.3	3.73
3.9	3.3	2.24	7.9	2.82	2.78	11.9	2	3.16	15.9	3.73	3.46	19.9	3.41	3.71
4	3.28	2.05	8	2.6	2.52	12	1.98	2.9	16	3.84	3.39	20	3.52	3.7

References

[1] M.W. Spong, S. Hutchinson, M. Vidyasagar, Robot modeling and control, IEEE Control Syst. 26 (2006) 113–115. doi:10.1109/MCS.2006.252815.

[2] A. Pott, Cable-Driven Parallel Robots, 2013. doi:10.1007/978-3-642-31988-4.

[3] J. Albus, R. Bostelman, N. Dagalakis, NIST SPIDER, a robot crane, J. Res. Natl. Inst. Stand. Technol. 97 (1992) 373–385. doi:10.6028/jres.097.016.

[4] M.J.-D. Otis, T.-L. Nguyen Dang, T. Laliberte, D. Ouellet, D. Laurendeau, C.M. Gosselin, Cable Tension Control and Analysis of Reel Transparency for 6-DOF haptic foot platform on a cable-driven locomotion interface, World Acad. Sci. Eng. Technol. 40 (2009) 520–532. doi:10.1016/j.ijpharm.2005.11.029.

[5] K. Usher, G. Winstanley, P. Corke, D. Stauffacher, R. Carnie, Air vehicle simulator: An application for a cable array robot, Proc. - IEEE Int. Conf. Robot. Autom. 2005 (2005) 2241–2246. doi:10.1109/ROBOT.2005.1570446.

[6] C.W.S.K. Hitoshi Kino, High-speed manipulation by using parallel wire-driven robots, Robotica. 18 (2000) 13–21.

[7] M. Hiller, S. Fang, S. Mielczarek, R. Verhoeven, D. Franitza, Design, analysis and realization of tendon-based parallel manipulators, Mech. Mach. Theory. 40 (2005) 429–445. doi:10.1016/j.mechmachtheory.2004.08.002.

[8] M. Gouttefarde, C.M. Gosselin, Analysis of the wrench-closure workspace of planar parallel cable-driven mechanisms, IEEE Trans. Robot. 22 (2006) 434–445. doi:10.1109/TRO.2006.870638.

[9] N. Zhang, W. Shang, S. Cong, Dynamic trajectory planning for a spatial 3-DoF cable-suspended parallel robot, Mech. Mach. Theory. 122 (2018) 177–196. doi:10.1016/j.mechmachtheory.2017.12.023.

[10] A. Pott, An Algorithm for Real-Time Forward Kinematics of Cable-Driven Parallel Robots, in: J. Lenarcic, M.M. Stanisic (Eds.), Adv. Robot Kinemat. Motion Man Mach., Springer Netherlands, Dordrecht, 2010: pp. 529–538.

[11] G. Barrette, C.M. Gosselin, Determination of the Dynamic Workspace of Cable-Driven Planar Parallel Mechanisms, J. Mech. Des. 127 (2005) 242. doi:10.1115/1.1830045.

[12] X. Diao, O. Ma, Vibration analysis of cable-driven parallel manipulators, Multibody Syst. Dyn. (2009). doi:10.1007/s11044-008-9144-0.

[13] B. Zhang, W. Shang, S. Cong, Optimal RRT* Planning and Synchronous Control of Cable-Driven Parallel Robots, 2018 3rd Int. Conf. Adv. Robot. Mechatronics. (2019) 95–100. doi:10.1109/icarm.2018.8610680.

[14] M.J.-D. Otis, T.-L. Nguyen-Dang, D. Laurendeau, C. Gosselin, Interference estimated time of arrival on a 6-DOF cable-driven haptic foot platform, in: 2009 IEEE Int. Conf. Robot. Autom., 2009. doi:10.1109/ROBOT.2009.5152182.

[15] R.G. Roberts, T. Graham, T. Lippitt, On the inverse kinematics, statics, and fault tolerance of cable-suspended robots, J. Robot. Syst. (1998). doi:10.1002/(SICI)1097-4563(199810)15:10<581::AID-ROB4>3.0.CO;2-P.

[16] M.J.D. Otis, S. Comtois, D. Laurendeau, C. Gosselin, Human safety algorithms for a parallel cable-driven haptic interface, in: Adv. Intell. Soft Comput., 2010. doi:10.1007/978-3-642-16259-6_15.

[17] B. Zi, B.Y. Duan, J.L. Du, H. Bao, Dynamic modeling and active control of a cable-suspended parallel robot, Mechatronics. (2008). doi:10.1016/j.mechatronics.2007.09.004.

[18] M.M. Aref, H.D. Taghirad, Geometrical workspace analysis of a cable-driven redundant parallel manipulator: KNTU CDRPM, in: 2008 IEEE/RSJ Int. Conf. Intell. Robot. Syst. IROS, 2008. doi:10.1109/IROS.2008.4650670.

[19] R. Meziane, P. Cardou, M.J.D. Otis, Cable interference control in physical interaction for cable-driven parallel mechanisms, Mech. Mach. Theory. (2019). doi:10.1016/j.mechmachtheory.2018.10.002.

[20] Y. Wischnitzer, N. Shvalb, M. Shoham, Wire-driven parallel robot: Permitting collisions between wires, Int. J. Rob. Res. (2008). doi:10.1177/0278364908095884.

[21] P. Tempel, F. Schnelle, A. Pott, P. Eberhard, Design and Programming for Cable-Driven Parallel Robots in the German Pavilion at the EXPO 2015, Machines. (2015). doi:10.3390/machines3030223.

[22] R.L. Williams, P. Gallina, Planar cable-direct-driven robots: Design for wrench exertion, J. Intell. Robot. Syst. Theory Appl. (2002). doi:10.1023/A:1021158804664.

[23] D.Q. Nguyen, M. Gouttefarde, On the improvement of cable collision detection algorithms, in: Mech. Mach. Sci., 2015. doi:10.1007/978-3-319-09489-2_3.

[24] R. Bordalba, J.M. Porta, L. Ros, Randomized kinodynamic planning for cable-suspended parallel robots, in: Mech. Mach. Sci., 2018. doi:10.1007/978-3-319-61431-1_17.

[25] M. Arsenault, Computation of the interference-free wrench feasible workspace of a 3-DoF translational tensegrity robot, in: Mech. Mach. Sci., 2019. doi:10.1007/978-3-030-20751-9_16.

[26] M. Fabritius, C. Martin, A. Pott, Calculation of the cable-platform collision-free total orientation workspace of cable-driven parallel robots, in: Mech. Mach. Sci., 2019. doi:10.1007/978-3-030-20751-9_12.

[27] T. Makino, T. Harada, Cable collision avoidance of a pulley embedded cable-driven parallel

robot by kinematic redundancy, in: Proc. 4th Int. Conf. Control. Mechatronics Autom. - ICCMA '16, 2016. doi:10.1145/3029610.3029620.

[28] M.J.D. Otis, S. Perreault, T.L. Nguyen-Dang, P. Lambert, M. Gouttefarde, D. Laurendeau, C. Gosselin, Determination and management of cable interferences between two 6-DOF foot platforms in a cable-driven locomotion interface, IEEE Trans. Syst. Man, Cybern. Part ASystems Humans. (2009). doi:10.1109/TSMCA.2009.2013188.

[29] S. Perreault, P. Cardou, C.M. Gosselin, M.J.-D. Otis, Geometric Determination of the Interference-Free Constant-Orientation Workspace of Parallel Cable-Driven Mechanisms, J. Mech. Robot. (2010). doi:10.1115/1.4001780.

[30] M. Ismail, S. Lahouar, L. Romdhane, Collision-free and dynamically feasible trajectory of a hybrid cable–serial robot with two passive links, Rob. Auton. Syst. 80 (2016) 24–33. doi:10.1016/J.ROBOT.2016.03.001.

[31] H. Simas, D. Martins, R. Di Gregorio, Smooth path planning for redundant robots on collision avoidance, in: Mech. Mach. Sci., 2019. doi:10.1007/978-3-030-20131-9_185.

[32] M. Lesellier, M. Gouttefarde, A bounding volume of the cable span for fast collision avoidance verification, in: Mech. Mach. Sci., 2019. doi:10.1007/978-3-030-20751-9_15.

[33] E. Moreira, A.M. Pinto, J.P. Sousa, J. Lima, P. Costa, A cable-driven robot for architectural constructions: a visual-guided approach for motion control and path-planning, Auton. Robots. 41 (2016) 1487–1499. doi:10.1007/s10514-016-9609-6.

[34] X. Zhou, C.P. Tang, V. Krovi, Cooperating mobile cable robots: Screw theoretic analysis, in: Lect. Notes Electr. Eng., 2013. doi:10.1007/978-3-642-33971-4_7.

[35] M. Anson, A. Alamdari, V. Krovi, Orientation Workspace and Stiffness Optimization of Cable-Driven Parallel Manipulators With Base Mobility, J. Mech. Robot. (2017). doi:10.1115/1.4035988.

[36] H. Tourajizadeh, M.H. Korayem, Optimal regulation of a cable suspended robot equipped with cable interfering avoidance controller, Adv. Robot. (2016). doi:10.1080/01691864.2016.1198719.

[37] E. Haug, Computer Aided Kinematics and Dynamics of Mechanical Systems, Allyn and Bacon, 1989.

[38] A.A. Shabana, Computational Dynamics, Third Edition, 2009. doi:10.1002/9780470686850.

[39] A. Ghasemi, M. Eghtesad, M. Farid, Neural network solution for forward kinematics problem of cable robots, J. Intell. Robot. Syst. Theory Appl. (2010). doi:10.1007/s10846-010-9421-z.

[40] A. El-Badawy, K. Youssef, On modeling and simulation of 6 degrees of freedom Stewart platform mechanism using multibody dynamics approach, in: Proc. ECCOMAS Themat. Conf.

Multibody Dyn. 2013, 2013.

[41] M.L. Husty, An algorithm for solving the direct kinematics of general Stewart-Gough platforms, Mech. Mach. Theory. (1996). doi:10.1016/0094-114X(95)00091-C.

[42] G. Liwen, X. Huayang, L. Zhihua, Kinematic analysis of cable-driven parallel mechanisms based on minimum potential energy principle, Adv. Mech. Eng. (2015). doi:10.1177/1687814015622339.

[43] T.F. Coleman, Y. Li, An Interior Trust Region Approach for Nonlinear Minimization Subject to Bounds, SIAM J. Optim. (1996). doi:10.1137/0806023.

[44] N. Sagara, M. Fukushima, A hybrid method for the nonlinear least squares problem with simple bounds, J. Comput. Appl. Math. (1991). doi:10.1016/0377-0427(91)90023-D.

[45] M. DEDIEU, J. P; SHUB, Newton's Method for Overdetermined Systems of Equations, Math. Comput. 69 (1999) 1099–1115.

[46] J.J. Moré, The Levenberg-Marquardt algorithm: Implementation and theory, (2006) 105–116. doi:10.1007/bfb0067700.

[47] C. Ericson, Real-Time Collision Detection, 2005. doi:10.1007/s13398-014-0173-7.2.

[48] C.B. Pham, S.H. Yeo, G. Yang, Tension analysis of cable-driven parallel mechanisms, in: 2005 IEEE/RSJ Int. Conf. Intell. Robot. Syst. IROS, 2005. doi:10.1109/IROS.2005.1545368.

[49] G. Boschetti, A. Trevisani, Cable robot performance evaluation by Wrench exertion capability, Robotics. 7 (2018). doi:10.3390/robotics7020015.

[50] G. Yang, C.B. Pham, S.H. Yeo, Workspace performance optimization of fully restrained cable-driven parallel manipulators, IEEE Int. Conf. Intell. Robot. Syst. (2006) 85–90. doi:10.1109/IROS.2006.281747.

[51] M. Gouttefarde, J.P. Merlet, D. Daney, Wrench-feasible workspace of parallel cable-driven mechanisms, Proc. - IEEE Int. Conf. Robot. Autom. (2007) 1492–1497. doi:10.1109/ROBOT.2007.363195.